UCSF

UC San Francisco Previously Published Works

Title

Mapping phospho-catalytic dependencies of therapy-resistant tumours reveals actionable vulnerabilities

Permalink

https://escholarship.org/uc/item/7gm1r4tn

Journal

Nature Cell Biology, 21(6)

ISSN

1465-7392

Authors

Coppé, Jean-Philippe
Mori, Miki
Pan, Bo
et al.

Publication Date

2019-06-01

DOI

10.1038/s41556-019-0328-z

Peer reviewed

Mapping phospho-catalytic dependencies of therapy-resistant tumours reveals actionable vulnerabilities

Jean-Philippe Coppé[1,*], Miki Mori[1,2], Bo Pan[1,3], Christina Yau[1], Denise M. Wolf[1], Ana Ruiz-Saenz[1], Diede Brunen[4], Anirudh Prahallad[4], Paulien Cornelissen-Steijger[5], Kristel Kemper[5], Christian Posch[1,6,7], Changjun Wang[1,3], Courtney A. Dreyer[1], Oscar Krijgsman[5], Pei Rong Evelyn Lee[1], Zhongzhong Chen[8,9,10], Daniel S. Peeper[4], Mark M. Moasser[1], René Bernards[4], Laura J. van 't Veer[1]

[1]Helen Diller Family Comprehensive Cancer Center, University of California, San Francisco, San Francisco, CA, USA. [2]Department of Breast Surgical Oncology, Showa University, Tokyo, Japan. [3]Department of Breast Surgery, Peking Union Medical College Hospital, Peking Union Medical College and Chinese Academy of Medical Sciences, Beijing, China. [4]Division of Molecular Carcinogenesis, Netherlands Cancer Institute, Amsterdam, the Netherlands. [5]Division of Molecular Oncology and Immunology, Netherlands Cancer Institute, Amsterdam, the Netherlands. [6]Department of Dermatology and Allergy, Technical University of Munich, Munich, Germany. [7]School of Medicine, Sigmund Freud University, Vienna, Austria. [8]The State Key Laboratory of Genetic Engineering, Collaborative Innovation Center of Genetics and Development, School of Life Sciences, Fudan University, Shanghai, China. [9]Ministry of Education Key Laboratory of Contemporary Anthropology, Collaborative Innovation Center of Genetics and Development, School of Life Sciences, Fudan University, Shanghai, China. [10]Present address: Department of Urology, Shanghai Children's Hospital, Shanghai Jiao Tong University, Shanghai, China.

Abstract

Phosphorylation networks intimately regulate mechanisms of response to therapies. Mapping the phospho-catalytic profile of kinases in cells or tissues remains a challenge. Here, we introduce a

---

[*] Jean-Philippe.Coppe@ucsf.edu.

practical high-throughput system to measure the enzymatic activity of kinases using biological peptide targets as phospho-sensors to reveal kinase dependencies in tumour biopsies and cell lines. A 228-peptide screen was developed to detect the activity of >60 kinases, including ABLs, AKTs, CDKs and MAPKs. Focusing on BRAF[V600E] tumours, we found mechanisms of intrinsic resistance to BRAFV[600E]-targeted therapy in colorectal cancer, including targetable parallel activation of PDPK1 and PRKCA. Furthermore, mapping the phospho-catalytic signatures of melanoma specimens identifies RPS6KB1 and PIM1 as emerging druggable vulnerabilities predictive of poor outcome in BRAF[V600E] patients. The results show that therapeutic resistance can be caused by the concerted upregulation of interdependent pathways. Our kinase activity-mapping system is a versatile strategy that innovates the exploration of actionable kinases for precision medicine.

In a functional sense, cancer is a proteomic disease that arises from selectively diverted signalling pathways[1–3]. While therapeutic decisions increasingly rely on the detection of mutated kinase genes or aberrantly expressed/phosphorylated proteins, few experimental platforms directly and comprehensively monitor the activity of kinase enzymes[4], and m any actionable dependencies of tumours often rem in undetected[5,6]. A technology capable of identifying the phospho-catalytic signatures of kinases in biological samples could improve therapeutic guidance, including dual-targeting strategies.

Proteomic detection systems use phosphorylatable regions of proteins to infer kinase activity. Antibody-based assays measure (phospho-)protein levels, which depend on the availability and specificity of antibodies[1,7–9]. Mass spectrometry techniques[10–17], somtimes combined with kinase inhibitors[18–21], allow the detection of raw amounts of (phospho-)proteins, but remain restricted due to cost, equipment and protocols. Alternatively, generic amino acid sequences are used as individual biochemical probes to directly detect kinases' phospho-catalytic activity in radioactive labelling assays, microfluidic electrophoresis systems, adenosine triphosphate (ATP) consumption tests, hybrid peptide/phospho-antibody platforms, or surface plasmon resonance (SPR) and fluorescence resonance energy transfer (FRET) techniques[22–29]. However, readouts from these approaches rely on broad-spectrum consensus peptides originally designed for one-probe-to-many-kinases detection methods, which are well suited for pharmacological drug screens, but not intended to specifically identify or differentiate between kinases' activity in biological extracts.

Here, we present a technological resource relying on collections of peptide probes, derived from biological target sites of kinases[30,31], that operate as distinct combinatorial peptide sets to distinguish and measure the phospho-catalytic activity of many kinases in parallel. The technology is modular by design: users can adapt probe libraries and assay conditions to their needs. Using a proof-of-concept 228-peptide library, we describe computational methods to analyse phospho-catalytic signatures established from high-throughput ATP consumption measurements. Using BRAF[V600E]-driven tumours as a test scenario, we demonstrate the utility of our approach by exploring and finding druggable kinase nodes that drive the unresponsiveness of colorectal cancer (CRC) and melanoma to anti-BRAF[V600E] therapy in cell models and patient tumours.

Results

Peptide-sensing platform to monitor phospho-signatures.

We sought to develop a high-throughput kinase activity-Mapping (HT-KAM) assay, hereby a compendium of peptides serves as combinatorial sensors of the phospho-catalytic activity of kinase enzymes. We synthesized a 228-peptide library (Supplementary Tables 1–3 and Supplementary Fig. 1a,b) that includes 151 biological 11-mer peptides corresponding to substrate protein regions variously phosphorylated by kinases involved in oncogenic processes[30]. The library also includes 14 generic 'positive control' (CON[+]) peptides commonly used as industry standards, and 63 reference peptides comprising 27 mutated, 31 pre-phosphorylated and 5 random peptide sequences. A liquid-dispensing instrument was programmed to aliquot peptide, sample, ATP and buffer solutions in 384-well plates (Supplementary Fig. 1c and Supplementary Table 4). Each well contained one peptide, and each plate simultaneously assessed the phospho-signature of one sample.

Multi-peptide-derived phospho-catalytic signatures distinguish individual kinases and their enzymatic subfamilies.

The phospho-catalytic activity profile of 25 recombinant kinases was measured in the presence of all 228 peptides (Fig. 1a, Supplementary Fig. 1d–l and Supplementary Tables 5 and 6). Inspection of kinase activity across all peptides revealed that each kinase displayed a unique phosphorylation fingerprint (Fig. 1a). Particular family members were functionally distinguishable from genetically related kinases (for example, the breast tumour kinase (BRK) or the src-related kinase lacking C-terminal regulatory tyrosine and N-terminal myristylation sites (SRMS) kinase versus the other Src family kinases (SFKs); or the mitogen-activated protein kinase 14 (MAPK14)/p38a versus MAPK1/extracellular signal-regulated kinase 2 (ERK2)), and the activities of kinase isoforms (LYN A versus LYN B) or oncogenic variants (Abelson murine leukaemia kinase 1 (ABL1) versus ABL1[T315I]) were discernible. Nevertheless, the principal factor clustering kinases was their family of origin (Fig. 1a,b).

We then examined how including a multiplicity of peptide sensors impacted the sensitivity and specificity of the assay for predicting the identity of an individual kinase. We computed area under the curve (AUC) values from repeated iterations of random peptide sampling. The sensitivity and specificity systematically improved when including an increasing number of peptides, while any single peptide performed poorly overall (Fig. 1c, Supplementary Fig. 2a–e and Supplementary Tables 7 and 8). For any given number of peptides, specific subsets performed significantly better than others, including kinases' biological peptides (Fig. 1d, red lines). For instance, for the haematopoietic cell kinase (HCK), the AUC derived from the specific combination of its eight biological peptide targets was higher than for most other eight-peptide combinations (Supplementary Fig. 2f).

Next, we asked whether our system could find peptide sets that best differentiate a kinase from others. We compared all phospho-catalytic profiles of kinases using a dual-significance threshold ($P < 0.05$ for a false discovery rate (FDR)-corrected F-test and Wilcoxon rank-sum test). This revealed that a unique differential phospho-signature could be systematically

assigned to every kinase (Fig. 1e,f and Supplementary Fig. 2g–j). Optimal signatures included every type of peptide (biological, generic CON[+] and reference) associated with both significantly high and significantly low phosphorylation activities. Thus, using a large spectrum of phospho-catalytic activity sensors enables a highly sensitive reporting system with which to differentially identify a specific kinase or kinase family.

Biological peptides are effective combinatorial activity sensors of their kinase enzymes.

We then asked whether kinases preferentially phosphorylate their respective biological peptides. We found that kinases were significantly more capable of phosphorylating the great majority of their biological peptide targets than control pools of 63 reference, 5 random or 16 Y/S/T-free peptides (Fig. 2a,b, Supplementary Fig. 3 and Supplementary Tables 9–12). Unsupervised clustering of kinases' activity using only biological peptides showed that biological peptides distinguished individual kinases, yet grouped them by functional relationships and kinase families (Fig. 2 c). Biological peptides contributed most to kinases' differential phospho-signature (Figs. 1e and 2 c and Supplementary Fig. 2g,h) and highest measurable activity (Supplementary Fig. 4).

These results show that biological peptides are excellent functional discriminators of kinases' phospho-catalytic signatures. Genetically distant kinases are distinguishable. Non-receptor tyrosine kinases are functionally defined as related. Yet, differences in the pattern and intensity of activity between members of the same kinase subfamily can be identified, which functionally shows what is so far inferred from differential protein-protein interactomes of distinct protein isoform s[32] (for example, LYN A/B) or family members (AKT2 and SRMS). This also shows that kinases affected by alternative splicing events or 'minimal' genetic/oncogenic mutations (ABL1T315I) can exhibit specific and distinctive phospho-catalytic activity profiles (as though encoded by unrelated genes), thus expanding the complexity of signalling networks and their alternative cancer states[30].

Computational analysis revealed that the phospho-catalytic signatures of kinases derived from their biological peptides outperformed generic CON[+] peptides and provided excellent specificity and sensitivity (average AUC> 0.9; Figs. 1d and 2d and Supplementary Fig. 2f,j). Noticeably, the somewhat lower AUC measured with SFK's biological peptides was attributable to specific differences in enzymatic properties between individual SRC family members (the AUC augments from 0.859 to > 0.92 when segregating SRMS, BRK, FGR and FRK, which behave as functionally distinct SFK subclass(es) and display little-to-no biological peptide overlap with other SFKs). This underlines the strict precision of the HT-KAM assay/analysis, and highlights how predictions based on functional distance between kinases' peptide phosphorylation signatures (instead of genetic proximity between kinase genes) could reshape enzymatic classifications and kinases' biological roles/druggability. Along with Fig. 1 d–f and Supplementary Figs. 2f–i, 3 and 4, the results in Fig. 2 indicate that biological peptide subsets are well-suited combinatorial sensors to specifically, sensitively, differentially and predictably detect the enzymatic activity of their respective kinases.

To further evaluate the performance of biological peptides as sensors of kinases, we measured the effect of kinase inhibitors. The activity profiles of ABL1, ABL[1T3151], LYNA

and AKT serine/threonine protein kinase 1 (AKT1) treated with the inhibitors dasatinib, imatinib and staurosporine showed that biological peptides effectively revealed the distinct drug sensitivities of kinases (Fig. 3a,b, Supplementary Fig. 5a–d and Supplementary Table 13). Statistical analyses showed that biological peptide sets systematically and significantly correlated with kinases' activity inhibition (Supplementary Figs. 4b and 5b–d). Similar results were found when measuring the effects of the SFK inhibitors PP2 and SU6656 on FYN, HCK, LCK and SRC (Supplementary Fig. 5e,f).

Along with Supplementary Figs. 4b and 5, the results in Fig. 3 show that biological peptides are adequate sensors to measure the activity of their cognate kinases (and are also practical because biological peptides are 'naturally occurring' targets derived from kinases' pools of specific protein substrates and target sites). Noticeably, for each kinase, the kinetics of responses to drug treatments are not exactly identical between the different peptides (for example, top left in Fig. 3a or Supplementary Fig. 5c, where the measurable effects of different imatinib concentrations on ABL1 activity depend on biological peptides; such repeatable peptide-to-peptide 'variations' are also detected with ABL1's set of commonly used generic CON[+] peptides). This suggests that kinases' differential avidity for (and phosphorylation of) particular peptide sensors is probably affected by inhibitors. This indicates that, to monitor the enzymatic functionality of a kinase, drug responses established from arrays of peptide probes could offer a level of confidence and precision that most single-peptide reporting assays would inherently lack. As such, the variety of biological peptides and control peptides included in our assay provides the enzyme-screening performance necessary to systematically identify, pare and validate kinases' activity profiles within and between technical replicates and samples of different compositions. Since the adaptability of our strategy allows for investigators to tailor peptide sensor libraries and enzymatic assay conditions to their needs, the assay and analytical methods we developed constitute a practical framework with utility towards pharmacological screens. Together, the results show that the identity and activity of kinases can be measured using their respective biological peptides.

Identifying druggable kinases that mediate intrinsic resistance to BRAF[V600E]-targeted therapy.

Providing a functional assay that identifies hyperactive, druggable kinases in cell culture models would be valuable to investigators. In the case of BRAF[V600E] CRC, finding effective targeted therapies has been a biomedical challenge. RNA interference screens performed in the WiDr cell line model originally found that parallel feedback activation of epidermal growth factor receptor (EGFR) caused intrinsic resistance to vemurafenib (VEM)[33–35]. Yet, patients' limited response to BRAF + EGFR combination therapy[36–38] underlines how crosstalk between signalling pathways often confounds genetic screen-drug response relationships[39]. We applied our assay to explore whether other kinases drive this unresponsiveness to BRAF therapy.

We used WiDr cells as a model system. WiDr cells treated with VEM displayed reduced mitogen-activated protein kinase kinase 1 (MEK1) and ERK2 kinase enzyme activity, and increased EGFR activity (Fig. 4a). This matched a reduction in the phospho-proteins

MEK1/2 and ERK1/2, and an increase in phospho-EGFR (Supplementary Fig. 6a–c), which confirmed that the HT-KAM assay could functionally replicate at the enzymatic level what is anticipated from the literature. We then concentrated on exploring additional targets. Examination of kinase signatures revealed that AKT1 was overly active, while its downstream tumour suppressor kinase, glycogen synthase kinase 3 beta (GSK3B), was inactivated (Fig. 4b). Furthermore, the activities of 3-phosphoinositid e-dependent protein kinase 1 (PDPK1) and its downstream effector kinases serum/glucocorticoid regulated kinase 1 (SGK1), protein kinase C alpha (PRKCA) and protein kinase N (PKN) were increased (Fig. 4b). Protein kinase D1 (PRKD1)—an effector of EGFR — was also upregulated (Fig. 4b). These changes in kinase activity Were significant (Fig. 4a–c and Supplementary Fig. 6d–f). Biological peptide subsets performed systematically better than generic CON$^+$ peptides in monitoring kinases' phospho-catalytic activity in cell extracts (Fig. 4a,b (red versus gold bars) and Fig. 4c), and were confirmed by immuno-detection (Supplementary Fig. 6f–h). These switches in kinases' functionality are cancer-promoting processes implicated in the cell cycle, survival and metabolism, suggesting that our assay functionally characterizes an adaptive drug response as the coordinated reprogramming of multiple, parallel signalling pathways.

To assess the role of these kinases as mediators of response and resistance to VEM, we tested the sensitivity of WiDr cells to drug combinations in cell survival assays. Besides AKT1, strong synergy was observed when BRAF^{V600E} targeting was paired with inhibitors of PDPK1 and PRKCA (Fig. 4d; colony formation validation for PDPK1 inhibition is shown in Fig. 4e). Conversely, inhibiting kinases found to be less active after VEM (ABL1, Janus kinase 2 (JAK2), c-Jun N-terminal kinase (JNK1) and p38a; Fig. 4b) remained ineffective (Fig. 4f), showing that HT-KAM offers an effective, logical framework to prioritize (and deprioritize) drug combinations with the highest likelihood of success. We validated the generalizability of these BRAF^{V600E} therapy resistance dependencies using additional kinase inhibitors and BRAF^{V600E} CRC cell lines (Fig. 4g, Supplementary Fig. 6h–j and Supplementary Table 14). The results show that our strategy can serve as a discovery platform to predict robust differences in kinase activity, and provide a rational design for combination therapies to target adaptive mechanisms of intrinsic resistance.

The phospho-catalytic signatures of cancer cells reveal their specific kinase dependencies.

Next, we asked whether our approach could be used to survey the activity of kinases across a panel of 20 cancer cell lines (Supplementary Fig. 6k,l and Supplementary Table 15). Figure 5a–d shows that all cancer cell lines could be systematically distinguished based on either their 228-peptide phosphorylation profiles (especially biological peptides) or their kinase activity signatures. The results in Fig. 5b,c show that biological peptides provide the broadest ranges and highest levels of measurable phosphorylation activities. Generic positive control peptides provide the lowest range of activities, and levels of phospho-activities remain lower than the overall mean activity per cell line across all cells. While virtually all peptides participate in defining the unique peptide phosphorylation activity signature of every cancer cell line, biological peptides are particularly Well-suited catalytic activity

sensors to measure and differentiate the unique functional phospho-fingerprint of cancer cells.

We then evaluated whether the differential kinase activities of these different cells could foretell their drug sensitivities. The results of com paring kinase activities measured using the kinases' biological peptide subsets versus GI_{50} concentrations for individual drugs (Fig. 5e and Supplementary Table 16) showed that the higher the activity of a proto-oncogenic kinase, the more a cell line was susceptible to responding to a matching drug. For instance, PC9 cells harbour an activating EGFR mutation, and their EGFR activity correlates with higher sensitivity to gefitinib compared with other cells (Fig. 5e, top left graph). We also found that cancer cells' drug sensitivities and their tumour of origin were best reflected when individual kinases' activities and comprehensive kinase activity signatures were derived from biological peptides, but not generic CON^+ peptides (Fig. 5f,g and Supplementary Fig. 6l,m).

As a specific biological question, we asked whether HT-KAM could identify kinases that functionally distinguish between baseline dependencies of $BRAF^{V600E}$ CRC and $BRAF^{V600E}$ melanoma by comparing WiDr and A375 cells (Fig. 5h and Supplementary Fig. 6n–p). We found that cyclin-dependent kinases (CDKs) and MEKs were significantly more catalytically active in A 375 cells than in WiDr cells, and A375 cells responded to much lower concentrations of the related drugs dinaciclib and trametinib. Hence, $BRAF^{V600E}$ cells of different tumour origins inherently relied on distinct kinase dependencies that were predictive of their drug sensitivities. Data for all 23 kinases and 35 inhibitors tested across 20 cell lines are com piled in Fig. 5i. Together, these results indicate that our platform provides a pragmatic solution to finding active, druggable kinases in cell culture models.

Mapping the phospho-catalytic signatures of patients' melanomas.

Identifying which kinases are overly active in patient tumours is of high clinical value. Malignant melanoma is a disease ultimately refractory to most current forms of therapy, including BRAF/MEK/ERK inhibitors used to treat metastatic $BRAF^{V600E}$ tumours[40–43]. Thus, we evaluated the potential utility of our assay in Mapping the phospho-catalytic signatures of patients' melanomas.

Nine surgically excised, fresh-frozen tumours from patients with melanom a were tested in four independent HT-KAM technical replicates (Supplementary Fig. 7a–c and Supplementary Tables 18 and 19). The 228-peptide phosphorylation signatures were analysed using unsupervised hierarchical clustering (Fig. 6a), principal component analysis (PCA; Fig. 6b) and dual-significance threshold selection (Fig. 6c and Supplementary Fig. 7a–c).

Figure 6b shows that survival and recurrence were highly associated with PC1/2, revealing the strong predictive and prognostic value of the peptide phosphorylation signature of tumours. Strong association between BRAF therapy-resistant lethal tumours and their phospho-signatures' PCs (outlined in red) validates the clustering results in Fig. 6a. Replicate runs from the same patient sample were significantly similar, whereas days on which assays were run were not associated with primary PCs of melanoma signatures,

showing the excellent performance and high reproducibility of the HT-KAM system (that is, experimental procedure, instrumentation and data analysis). The displayed PCA results were recapitulated when normalized with the 63 reference peptides, 16 Y/S/T-free peptides or 14 peptide-free tissue extracts alone, or when using raw ATP consumption data, showing the robustness of the strategy, as well as the reliability of its output in Mapping the phospho-catalytic signatures of tumours.

Together, the results in Fig. 6a–d show that the phospho-fingerprints of tumours were highly robust signatures that strongly associated with outcome (Fig. 6a–d, Supplementary Fig. 7d and Supplementary Tables 20 and 21). The group of signatures that retrospectively predicted poor outcome included all BRAF[V600E] tumours that did not respond to VEM (Fig. 6a,d (red squares) and Fig. 6b).

Next, we asked whether peptide phosphorylation profiles could reveal the hyperactive kinases of poor-outcome tumours. Figure 7a and Supplementary Fig. 7e–g show that kinase activity signatures established from biological peptides and compared across tumours were associated with outcome. Enrichment analysis using the most significantly and differentially phosphorylated biological peptides in poor-outcome patients showed that proto-oncogene serine/threonine protein kinase Pim (PIM), ribosomal protein S6 kinase B1 (RPS6KB) and AKT kinases were most active and more prevalent in poor-outcome melanomas, including VEM-resistant tumours (Fig. 7a,b, Supplementary Fig. 7f,h and Supplementary Table 22). G SK3B was significantly downregulated in these tumours (Fig. 7a,b). Hyperactive kinases suggest vulnerabilities that may be exploitable in the clinic.

We validated the prognostic value of the kinase hits discovered with HT-KAM by analysing > 400 melanoma patients&rsqo; data available from The Cancer Genome Atlas (TCGA)[44] (Fig. 7c). Furthermore, we confirmed that the concerted upregulation of PIM1, RPS6KB1 and AKT1 occurred in 36 BRAF[V600E] therapy-resistant patient-derived tumour xenografts (PDXs)[45] out of a cohort of 96 PDX melanoma patient tumours (Fig. 7d, e).Significantly more treatment-resistant PDXs display a combined increase in gene expression for any pair of PIM1, RPS6KB1 or AKT1 genes with a normalized z score > 0.5 $(X^2 < 0.007383$; Fig. 7d and Supplementary Table 23).

Translating kinase hits into therapeutic opportunities for BRAF[V600E] melanoma treatment.

On the basis of patient tumour kinase activity profiles found by HT-KAM screening (Fig. 7), we assessed the growth response of A375 and Sk-Mel-28 cells to kinase-targeting drug combinations. Figure 8a–c, Supplementary Fig. 8a–d and Supplementary Table 24 show that inhibitors of PIM, RPS6KB or AKT significantly potentiated the anticancer effects of BRAF inhibition, and outperformed mechanistic target of rapamycin kinase (mTOR) or MEK inhibitors whose effects in patients are variable and transient. In addition, other kinases whose catalytic activities were less highly and less significantly upregulated than PIM, RPS6KB or AKT in fatal BrAF[V600E] tumours were in fact less effective therapeutic targets, as exemplified by inhibitors of RPS6KA or protein kinase C (PKC) (additive effects only), and further confirmed in M el888 cells, whereas kinases whose activities were unchanged across patient tumours (for example, SRC) did not augment VEM sensitivity (Fig. 8d and Supplementary Fig. 8e). Furthermore, therapy-resistant/oncogenic mutant models derived

from A375 cells induced to exogenously express constitutively active AKT1(myrAKT1), MEK (MEK-DD) or SRC (SRC^{Y530F}) remained sensitive to RPS6KB or PIM targeting (Fig. 8d,e, Supplementary Fig. 8e–h and Supplementary Table 25), suggesting that these signalling hubs can function independently and in parallel, and represent suitable alternative targets to alleviate therapeutic resistance. Importantly, GSK3B inhibition antagonized VEM effects, thus mimicking a loss of tumour suppressive function by promoting resistance to BRAF therapy (Fig. 8a–e). The results support observations we made in patient tumours (Fig. 7a,b), where unresponsiveness to BRAF^{V600E} therapy was accompanied by coordinated inactivation of GSK3B and activation of PIM, RPS6KB and AKT kinases.

Finally, we investigated tumour cells, isolated from PDXs established from BRAF^{V600E} melanoma patients refractory to VEM[45], that maintained high levels of phospho-RPS6KB1 (Fig. 8f and Supplementary Fig. 8i–k). Colony formation showed that such tumours were particularly sensitive to RPS6KB inhibition. Thus, the activation of RpS6KB is a confirmed vulnerability that can be targeted to restore therapeutic sensitivity in BRAF therapy-resistant melanomas.

Discussion

A key to successful therapy is the identification of critical aberrant signalling networks whose inhibition would result in system failure of diseased cells. Here, we showcase the use of an innovative proteomic approach to identify specific kinase vulnerabilities that lie within the proto-oncogenic phospho-circuits of cancer cells and tumour tissues.

We developed a system that relies on collections of peptides to directly monitor the phospho-catalytic signatures of biological samples. Our strategy provides access to a vast, untapped resource of meaningful measurements, whether readouts are interpreted irrespective of which enzymes phosphorylate which probes, or analysed to convert global phospho-signatures into functional profiles of kinase activities.

In-depth computational analyses and systematic drug targeting of kinases established the advantages of our system to gain biological insights into signalling circuits. The combination of single phospho-activities measured across peptide sensors collectively distinguished the activity of different kinases with in or between samples of simple or complex com position (purified kinases, cells and tissues). Unlike other currently available kinase enzyme activity assays, the unique advantage of our approach is to use a multiplicity of peptides as combinatorial and differential sensors to measure the catalytic activity of kinases. Particular subsets of peptides (especially kinases' biological targets) provided superior sensitivity, specificity and discernibility over any single probe-derived measurement, including any individual generic CON$^+$ peptide used in current screening methods. The identity and activity of kinase enzymes across a broad range of kinase families could be simultaneously assessed from their respective subsets of biological peptides in various cancer cells and tumour tissues. The HT-KAM strategy is a versatile platform adaptable to users' needs (for example, interchangeable peptide libraries or assay conditions) and practical to both laboratory research and clinical settings.

We established that we could systematically deconvolute the peptide phospho-signatures of tumour cells to identify hyperactive, druggable kinases. We showed that the intrinsic and adaptive kinase dependencies of different tumours and cancer cells, including those harbouring an oncogenic BRAF^{V600E}, were distinctive and predictive of their drug sensitivity to single or com binatorial targeted therapies. HT-KAM functionally defined therapeutic resistance as the coordinated reprogramming of specific, parallel pathways. In CRC, the revealed kinase vulnerabilities driving VEM resistance in BRAF^{V600E} CRC cells included signalling cascades orchestrated by PDPK1, PRKCA and SGK1. In melanoma, PIM1 and RPS6KB1 were identified as druggable vulnerabilities predictive of poor outcome in BRAF^{V600E} patients.

These results suggest that drug resistance can result from a combination of pathways that are upregulated, working in concert and interdependent on each other, such that it requires their coordinated signalling activities to drive resistance. As such, the HT-KAM approach can identify a finite number of key cooperative dependencies, thus offering a highly selective choice of relevant targets to explore.

The fact that our assay identifies multiple kinases underlying drug resistance obviates the conventional approaches designed to sequentially identify individual drivers of collective resistance. Such a herd-like mode of resistance can only be discovered by the kind of mass-scale functional proteomic approach we have developed.

In particular, our approach effectively identified targets beyond those previously found by synthetic lethality genetic dropout screens or gene overexpression systems in the same CRC[33] or melanoma[46] cell models, and without requiring laborious, exogenous genetic interventions that inevitably alter signalling circuits. Instead, our platform is an analytical platform, not an experimental system, that can directly be applied to the interrogation of tumour biospecimens or cells in their native state. Moreover, not all genes found by genetic screens are druggable, whereas identifying hyperactive kinases represents the most proximal readout of actionable targets, significantly increasing the translational impact of discoveries. Furthermore, large-scale gene expression/mutation analyses would not identify the targets that HT-KAM found because no evident genetic alterations have been reported for these genes in cell lines or patient tumours (for example, PDPK1 or PRKCA in BRAF^{V600E} CRC or RPS6KB1 in BRAF^{V600E} melanoma)[12,30,42,44,45] Also, the results from considerable genomic study efforts suggest that, for many cancers, including CRC, therapeutic resistance is probably not driven by individual genetic dependencies or caused by a unique driver mutation.

Additionally, studies relying on antibody arrays and mass spectrometry proteomic approaches did not find the targets discovered with HT-KAM. Protein quantification tools can only indirectly infer the functional state of proteins and cannot directly measure the levels of catalytic activity of enzymes or kinases, which is what most targeted therapies are designed to inhibit if or when they are aberrantly hyperactive[3,47,48]. Hence, the readouts from our innovative system do not overlap with the results from current proteomic technologies, and instead offer a unique opportunity to reveal a molecular depth that complements these other platforms to better understand the mechanisms of diseases.

Functional proteomic platforms designed to detect the activity of kinase enzymes (and eventually the functionality of the whole kinome), such as HT-KAM, are missing from the current biotechnology landscape, yet are really needed to start elaborating the functional m aps of signalling networks that can directly pinpoint actionable vulnerabilities of tumours. Such strategies may initiate a paradigmatic shift in our comprehension of cell and tissue responses to drug interventions and therapeutic resistance.

From a clinical standpoint, knowledge of how to choose and pair limitless combinations of drugs has become a pressing need for pharmaceutical industries and physicians who grapple with treatment resistance in patients[39,49,50]. The HT-KAM platform provides a rational design to help prioritize (and de-prioritize) drug combinations and maximize the likelihood of success (for example, RPS6KB proto-oncogenic kinase versus GSK3B tumour suppressor kinase). Furthermore, the peptide phosphorylation signatures discovered here represent a yet-unexplored parameter that has the potential to be configured into diagnostic tests, especially since we showed using computational analyses that it will be possible to build 'fit-for-purpose kits' relying on narrow sets of best-predictor peptides customized to monitor the activity of particular kinases for research or diagnostic purposes. For instance, BRAF^{V600E} melanoma patients who retrospectively displayed phospho-signatures indicative of aggressive disease may have benefited from targeting BRAF+RPS6KB1 or PIM1, instead of standard therapies on which patients almost inevitably relapse. Some of the diagnosable susceptibilities we uncovered represent therapeutic alternatives that may be tested in the clinic. Since kinase circuits are probably cell/patient specific, it will become important to profile the kinome signatures of individual patients' tumours to personalize medical treatments.

In conclusion, combinatorial peptide-sensing systems constitute an effective way to capture the functionality of kinase enzymes in cells and tissues. Such a modular strategy addresses a central challenge in the biomedical field, and could play an integral role in improving research productivity and guiding therapeutic decisions. Mapping the phospho-catalytic signatures of diseases innovates the molecular exploration of signalling networks and supports the discovery of actionable dependencies for precision m edicine.

Methods

Kinase enzyme activity assay.

The phospho-catalytic signature of samples was established from simultaneously occurring ATP consumption tests measured in the presence of peptides that were experimentally isolated from each other in multi-well plates. Assays were run in 384-well plates (solid, white flat-bottom plates; Corning; catalogue number: 3570), where each experimental well contained one type of peptide. The final 8 μl reaction mixtures per well contained the following final concentrations of reagents: (1) 1x kinase assay buffer (prepared daily and diluted in double-distilled water from a 10x stock solution of 25 mM Tris-HCl (pH 7.5), 10 mM MgCl$_2$, 0.1 mM Na$_3$VO$_4$, 5 mM β-glycerophosphate and 2 mM dithiothreitol, or purchased from Cell Signaling Technology; catalogue number: 9802); (2) 250 nM ATP (prepared from a 10 mM stock solution of adenosine-5'-triphosphate in double-distilled water and diluted daily with 1x kinase assay buffer; Cell Signaling Technology catalogue

number: 9804); (3) 200 μg ml^{-1} 11-mer peptide (lyophilized stocks originally prepared as 1 mg ml^{-1} in 1x kinase assay buffer and 5% dimethyl sulfoxide); and (4) samples typically made of either 5 ng μl^{-1} recombinant kinase enzyme protein or 10 μg ml^{-1} protein extract from cell or tissue lysates (see below for the protocol) that were kept on ice and diluted in 1x kinase assay buffer <30m in before experimental testing. Controls with no ATP, no peptide or no sample, as well as ATP standards, were run side by side within each 384-well plate.

High-throughput liquid dispensing of all reagents was achieved using the Biomek FX Laboratory Automation Workstation from Beckman Coulter (hosted by the Center for Advanced Technologies at the University of California, San Francisco), and was programmed to specifically address the dispensing requirements of the assay (timing, sequence, tip-touch location, height and depth, and so on). Accurate dispensing was thoroughly and regularly validated. All reagents were kept on ice and plates were kept on cold blocks (VWR/BioCision; CoolRack × T PCR96 (catalogue number: 89239–498) and CoolSink XT 96F (catalogue number: 89239–504)) until enzymatic reactions were started. For all intermediary steps over the course of the assay (that is, buffer and sample preparation, dispensing, and so on), we used microcentrifuge tubes (Costar; catalogue number: 3621) and clear 96-well PCR-plates (V W R; catalogue number: 83007–374).

Once the dispensing of reaction mixtures was completed, 384-well reaction plates were typically incubated for 30 min at 30°C. After enzymatic reactions were completed, the final detection step used Kinase-Glo revealing reagent (Promega; catalogue number: V3772; dispensed using a Biomek Automated Workstation), which stopped the activity of the kinase enzymes and produced a luminescent signal directly correlated with the amount of remaining ATP in the samples over a broad range of ATP concentrations (the repeatability and accuracy of the ATP-dependent luminescence assay measurements were tested and validated over 5 logs of ATP standard concentrations; R^2 (coefficient of determination) > 0.99, and measurements from the large variety of peptides offered a broad dynamic range of measurable catalytic activities (over 4 logs of magnitude) that were observable for each individual kinase and between different kinases). Luminescence was inversely correlated with the amount of kinase activity. Luminescence was measured using the Synergy 2 Multi-Mode Microplate Reader from BioTek, and occasionally the Molecular Devices Analyst AD microplate reader from McKinley Scientific. We systematically checked that all samples' ATP profiles fitted within the limits of the range of the ATP standard and that no evidence for any ATPase or phosphatase contamination was present, hence allowing for activity profiles to be interpreted with confidence, and for measurable variations in phospho-catalytic activities measured in the presence of peptides to be considered as both peptide dependent and cell, tissue or kinase specific.

Peptide sensors.

11-mer amino acid sequences were made to order and mass synthesized by GenScript at >95% purity. The 228-peptide library included 151 biological peptides, 14 generic CON$^+$ peptides and 63 reference peptides that included 27 mutated (tyrosine (Y)/serine (S)/ threonine (T) →glycine (G)) and 31 pre-phosphorylated (Y/S/T → pY/pS/pT) peptides, as well as 5 random peptide sequences (Supplementary Table 1 provides the peptide sequence

details and connectivity between peptides and kinases). Biological peptides corresponded to phosphorylatable amino acid regions of substrate protein identified from the literature and curated in resources such as PhosphoAtlas[30] (Supplementary Fig. 1a,b; http:// cancer.ucsf.edu/phosphoatlas) or Phospho Site Plus[31]. Each generic CON[+] peptide corresponded to a kinase activity-reporting probe commonly used in single-peptide assays as available/advertised from the literature or manufacturers, and may have corresponded to a commonly known 'consensus' amino acid sequence. As such, biological peptides and generic CON+ peptides could be classified as 'predicted' or not (that is, 'other'); for instance, in Fig. 1e, where 'predicted' defines a peptide previously identified in the literature as a target of a given kinase (that is, an amino acid sequence corresponding to a known phosphorylatable protein region for a biological peptide[30] and a commercially available amino acid sequence advertised as a kinase probe/sensor for a CON[+] peptide). Some of the generic positive control peptides were purchased from SignalChem (for example, Abltide (catalogue number: A 02–58) and Poly (4:1 Glu, Tyr) peptide (catalogue number: P61–58)). Biological peptides were selected based on the sentinel cancer-regulating role of their kinase-substrate target sites, as identified in PhosphoAtlas[30].

Recombinant kinases.

The following purified, recombinant kinase enzymes were purchased from SignalChem: ABL1/c-ABL (catalogue number: A03–18H), ABL1[T31SI] (catalogue number: A03–12D G), ABL2/ARG (catalogue number: A04–11H), AKT1/PKB/RAC (catalogue number: A 16– 10G), AKT2 (catalogue number: A 17–10G), AKT3 (catalogue number: A 18–10G), BLK (catalogue number: B02–10G), BRK/PTK6 (catalogue number: P94–10G), CSK (catalogue number: C63–10G), EGFR/human epidermal growth factor receptor 1 (HER1) (catalogue number: E10–11G), ErbB2/HER2/NEU (catalogue number: E27–11G), ErbB4/HER4 (catalogue number: E29–11G), ERK2/MAPK1/p42 (catalogue number: M28–10G), FGR (catalogue number: F10–10G), FRK (catalogue number: F14–11G), FYN isoform A (catalogue number: F15–10G), FYN isoform C (inactive; catalogue number: F15–14G –20), HCK (catalogue number: H02–11G), JAK2 (catalogue number: J02–11H), LCK (catalogue number: L03–10G), LYN isoform A (catalogue number: L13–18G), LYN isoform B (catalogue number: L13–10G), p38a/MAPK14 (catalogue number: M 39–10BG), SRC/c-SRC (catalogue number: S19–18G), SRM/SRMS (catalogue number: S20–11G) and YES/ YES1 (catalogue number: Y 01–10G). The same concentration of every kinase was used in all experiments (Figs. 1–3 and Supplementary Figs. 1–5).

Kinase inhibitors.

The following inhibitors were used in biochemical assays or cell culture. Inhibitors purchased from Selleck Chemicals were: 1-Azakenpaullone (catalogue number: S7193), AT13148 (catalogue number: S7563), AZD1208 (catalogue number: S7104), AZD7762 (catalogue number: S1532), BAY-61–3606 (catalogue number: S7006), BI-D 1870 (catalogue number: S2843), bosutinib/SKI-606 (catalogue number: S1014), BX-912 (catalogue number: S1275), CI-1040/PD184352 (catalogue number: S1020), C ID 755673 (catalogue number: S7188), CH IR-99021 (catalogue number: S1263), dasatinib (catalogue number: S1021), dinaciclib/SCH-727965 (catalogue number: S2768), everolimus/RAD001 (catalogue number: S1120), fedratinib/SAR302503 (catalogue number: S2736), gefitinib/

ZD-1839 (catalogue number: S1025), G o-6983 (catalogue number: S2911), GSK2334470 (catalogue number: S7087), G SK650394 (catalogue number: S7209), H89 (catalogue number: S1582), imatinib (catalogue number: S1026), IPA-3 (catalogue number: S7093), JNK Inhibitor V III (catalogue number: S4901), LFM-A13 (catalogue number: S7734), LY2584702 (catalogue number: S7704),M K 2206 (catalogue number: S1078), nilotinib/ AMN-107 (catalogue number: S1033), OSU −03012 (catalogue number: S1106), pelitinib/ EKB-569 (catalogue number: S1392), PLX-4720 (catalogue number: S1152), PF-4708671 (catalogue number: S2163), ponatinib/AP24534 (catalogue number: S1490), RO −3306 (catalogue number: S7747), ruxolitinib/INCB018424 (catalogue number: S1378), saracatinib/AZD0530 (catalogue number: S1006), selumetinib/AZD6244 (catalogue number: S1008), sotrastaurin (catalogue number: S2791), SP600125 (catalogue number: S1460), TAK-715 (catalogue number: S2928), trametinib/GSK1120212 (catalogue number: S2673), VEM/PLX4032 (catalogue number: S1267) and V X-702 (catalogue number: S6005). Inhibitors obtained from other companies were A S601245 (Cayman; catalogue number: 17542), bryostatin 1 (Sigm a-Aldrich; catalogue number: B7431), PP2 (Invitrogen; catalogue number: PH Z1223), PP3 (Tocris; catalogue number: 2794), SL 0101–1 (Tocris; catalogue number: 2250), staurosporine (Sigm a-Aldrich; catalogue number: S4400) and SU6656 (EMD/Calbiochem; catalogue number: 572635). The conditions of use are indicated in the text (except for data on cell lines' sensitivity to the N PK76-ii-72–1 inhibitor, which were derived from Garnett et al.[52] and used to validate the HT-KAM-predicted activity of polo-like kinase (PLK)). IC_{50} and GI_{50} correspond to the concentrations of a given drug that cause 50% inhibition of kinase activity (IC_{50}) or cell growth (GI_{50}).

Cell culture, and cell viability, cell death and colony formation assays.

The cells used in this study included cell lines, primary PDX tumour cell lines, drug-treated cells and genetically modified cell lines. The cancer cell lines used in this study were purchased from the American Type Culture Collection or provided by the laboratories of R.B., S. Ortiz-Urda, M. Bissell or F. McCormick (CRC: WiDr, HT29, SK-CO-1, HCT116, RKO −1, LIM2405, KM20 and Colo-205; melanoma: A375, A375 myrAKT1, A375 M EK-DD, A375 SRC^{Y530F}, A375 controls (A375 pCON empty vector and A375 SRC wild type), Sk-Mel-28, Mel888, MM 485 and Sk-Mel-2; lung: H1755, H3122 and PC9; breast: AU565, HCC70, MCF7, MDA-MB-231,MDA-MB-436, T47D, HMT-3522 S1 and HMT-3522 T4; prostate: PC-3; and thyroid: 8505C), from which 15 lines were BRAF^{V600E} mutated (WiDr, HT29, RKO-1, LIM2405, KM 20, Colo-205, A375 (plus five oncogenic/therapy-resistant variants of A 375), Sk-Mel-28, Mel888 and 8505C), 2 melanomas were *NRAS* mutated (MM485 and Sk-Mel-2) and 2 CRCs were *KRAS* mutated (SK-CO-1 and HCT116). Cells were cultured following the American Type Culture Collection's instructions or as previously described[33].

We used primary melanoma cell lines established in previously performed studies[45,53] (that is, no cell line derivation processes and no animal experiments were directly performed over the course of this study). The cell lines we used were identified as M032R6.X1.CL and M061R.X1.CL, and were previously described and derived from therapy-resistant BRAF^{V600E} melanoma PDXs respectively identified as M032R6.X1 and M061R.X1 (refs. 45,53).

To assess the growth/survival response of cell lines to single or combinatorial drug treatments (Figs. 4, 5 and 8 and Supplementary Figs. 6 and 8), we used a CellTiter-Glo cell viability assay (Promega; catalogue number: G7571). Cell culture and luminescence readouts were performed in 96- and 384-well plates after 3-day treatments. The effects of drug combinations on cell growth were assessed by calculating the drug interaction (two-way analysis of variance (ANOVA) using Prism or SigmaPlot software) and combination index (following either: (1) the Loewe additivity m odel[54–56] and arbitrary threshold (synergy: combination index < 0.6; additivity: 0.6 < combination index < 1.0; antagonism: combination index > 1); or (2) the Bliss independence model[57–59], which uses experimental profiles avoiding inaccuracies from dose-effect curve estimations, and is calculated as combination index = $\log_2[E_{a,b}/(-E_a \times E_b)]$, where E_a and E_b correspond to the effects of drugs A and B alone at a given concentration, and E a,b corresponds to the combined effects of drugs A and B at the same concentration, and a combination index of <0 indicates synergy while a combination index of > 0 relates to an antagonistic effect). We systematically tested the effects of drugs in both regular and low-serum culture conditions (that is, 5.00 and 0.25% foetal bovine serum (FBS) media). Specifically, in the left panel of Fig. 4g, characteristics of the response to drug combinations are provided as colour-coded squares underneath each corresponding bar of the graph, where the combination index follows the Loewe additivity model and was measured as the average growth inhibition for VEM < 2μM and a second drug concentration of < GI_{50}. For the right panel of Fig. 4g (heat map) and the colour-coded banners underneath the graphs in Fig. 8d and Supplementary Fig. 8e, combination index values were derived from the Bliss model and averaged from values for nine individual combination indices experimentally measured around drugs' GI_{50} (that is, at GI_{50}, $2 \times GI_{50}$, $0.5 \times GI_{50}$ concentrations of each drug).

To generate the results in Fig. 5e,g and Supplementary Tables 16 and 17, we tested the effects of 27 kinase-inhibiting drugs in 3-day dose-response cell viability assays using a core set of cell lines (A375, AU565, H3122, HCC70, HCT116, HT29, MCF7, MDA231, MDA436, SK-CO-1, SkMel2, T47D and WiDr; additional cell lines were tested on a case-by-case basis where it was deemed useful, such as PC9 to compare EG FR activity versus gefitinib sensitivity[60]). We intentionally chose to test more than one inhibitor per kinase for some of the kinases to validate the results: the 27 drugs inhibit 20 different kinases/kinase families. We alsofurther corroborated GI_{50} results from the literature[52,61,62]. Kinase activity levels were extracted from the signatures available in Fig. 5d and Supplementary Fig. 6l,m (that is, kinase activities calculated from kinases' biological peptide subsets (or CON+ peptide subsets) extracted from much larger arrays of peptide phosphorylation profiles). We then correlated cancer cells' GI_{50} values with their kinase activity for each drug, thus allowing us to evaluate the performance and biological relevance of the HT-KAM assay. The results for the PLK inhibitor NPK76-ii-72–1 were derived from HT-KAM-derived PLK activity levels (computed in Supplementary Fig. 6l) and compared with GI_{50} profiles available from the literature[52]. A negative correlation between kinase activity and drug GI_{50} values across cells indicated that, overall, cell lines were more susceptible to inhibitors for which they displayed higher proto-oncogenic kinase activity, such as AKTs or SFKs. (In principle, the opposite would happen when blocking a kinase with tumour-suppressive activity; for example, GSK3B.) The goal of this method was to assess whether profiles

measured by HT-KAM assays accurately predict differences in kinase activity, and whether HT-KAM screening makes it possible to find kinases with higher activity levels and higher likelihood of responding to kinase-targeting drugs. It may also be used to identify unanticipated outliers with exploratory value in alternative signalling cascades and drug treatments.

In Fig. 5i, the differential kinase activities and drug GI_{50} values were first compared for each kinase-drug pair across tested cancer cell lines (as shown in Fig. 5e and Supplementary Fig. 6n). Then, the differential profiles were pooled across all tested kinase-drug pairs.

To quantitate cell death (Fig. 8 and Supplementary Fig. 8), fluorescence-activated cell sorting analysis of nuclear degradation was performed as previously described[63]

Colony formation assays (Figs. 4 and 8 and Supplementary Fig. 8) were performed as previously described[45].

Preparing protein lysates from cell lines for kinase assay.

To measure the phospho-catalytic activity of cancer cell lines (Figs. 4 and 5 and Supplementary Fig. 6), cultured cells were lysed for 5 min in ice-cold cell lysis buffer. Freshly prepared lysis buffer (1 ml per 5.10^6 cells) contained non-denaturing Cell Lysis Buffer 1x (diluted in double-distilled water from 10x stock of 20 mM Tris-HCl (pH 7.5), 150 mM NaCl, 1 mM Na2EDTA, 1 mMEGTA, 1% Triton, 2.5 mM sodium pyrophosphate, 1 mM β-glycerophosphate, 1 mM Na_3VO_4 and 1μg ml^{-1} leupeptin, or purchased from Cell Signaling Technology (catalogue number: 9803)), complemented with 1x Halt Protease and Phosphatase (Therm ofisher Scientific (catalogue number: 1861281), which contains inhibitors of Ser/Thr phosphatases and Tyr phosphatases). Scraped off lysates were then spun down at 14,000 r.p.m. in a cold/+4°C centrifuge for 15 min, and supernatants were systematically stored at −80°C. When experiments were performed at the Netherlands Cancer Institute, samples were shipped on dry ice to the University of California, San Francisco. Protein and ATP concentrations were quantified. Since every HT-KAM assay plate includes 14 wells with sample alone (that is, without peptide), internal controls for ATP levels were systematically available for all assays/samples. To test the kinase activity responses of the WiDr cell model to VEM (Fig. 4a–c and Supplementary Fig. 6 a–f), cells were treated as previously described[33].

Tumour specimens from melanoma patients.

Biospecimens were collected in a separate study being performed independent of the present work. Briefly however, patient samples were collected at the Rudolfstiftung Hospital (Vienna, Austria) and University of California, San Francisco (United States) under the Institutional Review Board numbers 13–204-VK and 12–09483, respectively. The study was compliant with all relevant ethical regulations regarding research involving human participants, and informed consent was obtained from all participants. Sample collection was in line with the declaration of Helsinki and Good Clinical Practice, and was reviewed by the Ethical Committee of the City of Vienna. Clinical details regarding patients are available in Supplementary Table 18. Within the group of deceased patients (that is, poor-outcome patients 2, 4, 5, 8 and 9), patients 4, 5 and 9 were VEM resistant, patients 2, 4 and 8 were

ipilimumab resistant, and patient 2 was BRAF[V600E] negative. Within the group of surviving patients (that is, good-outcome patients 1, 3, 6 and 7), patients 3 and 7 were BRAF[V600E] positive, and patient 3 initially recurred/relapsed. Tumour tissues not needed for diagnostic purposes were collected intraoperatively, macroscopically dissected and flash frozen. A small piece of tumour tissue was embedded in Optimal Cutting Temperature compound, sectioned, stained with haematoxylin and eosin and analysed to ensure >80% tumour cell content in the tumour tissue samples.

Preparing protein lysates from tumour tissues for kinase assay.

Flash-frozen melanom a tissue specimens were pulverized using a BioSpec 59012MS instrument. Protein extracts from powdered samples were prepared following the lysis protocol used for cultured cells (see above). All samples were stored at −80°C. Internal controls for ATP levels in peptide-free wells were systematically measured (see Supplementary Fig. 7b and Supplementary Table 19). The total amount of tumour tissue sample necessary to profile the activity of kinases across 384-well plates ranged from 20–30 μg (which is less than the typical 100 μg collected per core biopsy).

TCGA data analysis.

Messenger RNA data from melanoma specimens available from the TCGA resourcet142[44] (TCGA Research Network: http://cancergenome.nih.gov/) were analysed to identify samples with altered gene expression compared with reference samples using a z-score cut-off of ± 2 (shown in Fig. 7c). The z-score was defined as (expression in tumour sample − mean expression in reference sample)/(s.d. of expression in reference sample), where the reference population was either all tumours that were diploid for the gene in question or, when available, normal adjacent tissue.

BRAF[V600E] melanoma PDXs.

We used samples that were collected in a previously performed study[45,53] (that is, no animal experiments took place over the course of the present study). For information regarding melanoma PDXs and BRAF therapy (VEM)-resistant models, please refer to previous work by Kemper and colleagues[45,53]. The collection and use of human tissue was approved by the Medical Ethical Review Board of the Antoni van Leeuwenhoek Hospital (Amsterdam, the Netherlands). Animal experiments were approved by the animal experimental committee of the Netherlands Cancer Institute and performed according to Dutch law. This study was compliant with all relevant ethical regulations regarding animal research. As a validation of the phospho-catalytic profiles defined by the HT-KAM platform and the kinase hits we found in patients' biospecimens, we analysed tissue extracts from 96 PDXs including 36 BRAF therapy-resistant patients/PDXs for gene expression (see Fig. 7d and raw RNA sequencing (RNA-Seq) data available in Supplementary Table 26; RNA-Seq data were generated by O. Krijgsman et al., manuscript in preparation) and protein expression (Fig. 7e).

Statistics and reproducibility.

Below, we provide general information on how statistical analyses of the data were conducted, and general information on the reproducibility of the experiments. We specifically concentrate on details of the analysis of phospho-catalytic profiles, as well as the statistical methods, logical steps and computational tools developed to analyse the peptide phosphorylation profiles and kinase activity signatures (further complementing explanations are available in the main text and Supplementary Information).

Normalization methods were used to transform raw ATP consumption measurements into interpretable peptide phosphorylation profiles. First, for biochemical samples (Figs. 1–3 and Supplementary Figs. 1–5), the average value of ATP consumption across 228-peptide sensors for each experimental run was systematically used for internal normalization of each experimental run. To further analyse and cross-validate the output of these results, we also used three other normalization schemes relying on specific peptide sensor subsets: (1) 63 reference peptides; (2) 16 Y/S/T-free peptides; or (3) 5 random peptides. Second, for cell or tissue samples (Figs. 4–7 and Supplementary Figs. 6 and 7), the average value of ATP consumption across the 228 peptides and 14 data points from cell/tissue extract alone (that is, established from 14 peptide-free control wells per 384-well plate) was systematically used for internal normalization of each experimental run. We further analysed and cross-validated these results using the subsets of: (1) 14 peptide-free control wells (that is, cell or tissue extract alone); (2) 16 Y/S/T-free peptides; or (3) 63 reference peptides. The results of these different normalization schemes for either biochemical samples, cell extracts or tumour tissue extracts were then subjected to statistical and comparative analyses, as described elsewhere in the text.

Methods to compare phospho-signatures between samples were implemented. First, readouts from normalized peptide phosphorylation profiles were compared using statistical analyses and predictive methods, allowing profile analyses and interpretations irrespective of which kinase enzymes phosphorylate which probes. Second, for the kinase signature profiles, the activity of the kinases was calculated as the average of the phosphorylation activities measured in the presence of their respective biological peptide subsets. This defines how peptide libraries can be used as combinatorial sensors of enzymes' activity to convert complex peptide phosphorylation profiles into kinase activity signatures. Here, we systematically analysed cell/tumour kinase signatures for individual kinases or kinase families detected with > 4 biological peptides available in the 228-peptide library used in this study (that is, 60 kinases). Statistical analyses and predictive methods were then applied to compare kinase activity profiles between cancer cell extracts and tumour tissue samples. As the HT-KAM platform was intentionally designed as a modular system, investigators may adapt it to their needs using different, larger or smaller probe libraries, or different assay conditions, normalization, analytical processes or deconvolution strategies (for example, numbers of peptide sensors per kinase, *P* value thresholds, and so on).

In the analysis of AUC progression profiles in Fig. 1c and Supplementary Fig. 2a,b, the 'outcome' we wanted to predict was the identity of a kinase based on peptide phosphorylation profiles. For example, for AKT, the outcome of the analysis was 'does this activity profile belong to the AKT family: yes or no?' when using activity profiles from one

or multiple peptides that were randomly drawn from any of the 228 peptides, then comparing the activity profiles derived from the same peptide set across all recombinant kinases and all experimental repeats. To do so, diagonal linear discriminant analysis (DLDA) class predictors were built for each kinase (or kinase family) using randomized combinations of an increasing number of peptides to discriminate one given kinase (or kinase family) from all others. The performance of the DLDA classifier was defined as the AUC (that is sensitivity and specificity) for predicting the identity of a kinase (or kinase family) from repeated iterations $(i = 1,000)$ of random peptide sampling. The confidence intervals of AUCs were computed using the DeLong method (from the pROC package of R). In Fig. 1c and Supplementary Fig. 2a,b, graphs of AUC values $(y$ axes) obtained for any number (n) of combined peptides $(x$ axes) show AUC progression profiles as box plots. Plots show the effect of increasing n on AUC values, where n random peptides are drawn from 228 peptides, and where n spans from 1 to a combination of 50 peptides (Fig. 1c and Supplementary Fig. 2a) or from 1 to a combination of 100 peptides (Supplementary Fig. 2b). We chose to analyse individual kinases for which enough experimental repeats were executed (stringent cut-off > 6 repeats; that is, ABL1, AKT1, EGFR, ERK2, p38a, HCK and SRC), and kinase families with sufficient (> 6) repetitions across individual kinases belonging to each family (that is, ABL, AKT, HER, MAPK and SFK). Such a method answers: (1) how does including an increasing number of combined peptide sensors impact the sensitivity and specificity of a kinase assay intended to measure a kinase's phospho-catalytic activity?; (2) can particular subsets of peptides perform significantly better than other combinations within a particular iterative number of peptides? (that is, higher AU C's within a given number of peptides)?; and (3) can we find some unique combinations of fewer peptides that behave as highly specific and sensitive reporters of a given kinase? (that is, peptide subsets would be located towards the top left corner of each plot in Fig. 1c and Supplementary Fig. 2a,b). However, this method cannot find which combinatorial set of peptides would differentiate (with the highest probability and specificity/sensitivity) between a kinase and other kinases, which is a question resolved with the method developed for Fig. 1e,f and Supplementary Fig. 2g–i.

For the analysis in Fig. 1e and Supplementary Fig. 2g,h, we implemented computational methods to define which unique set of peptides most significantly distinguishes a kinase from all other kinases. The first step of the analysis was to systematically compare each of the 228-peptide activity signatures of an individual kinase (or all kinases belonging to a given family) with > 6 experimental repeats (that is, ABL1, AKT1, EGFR, ERK2, p38a, HCK, SRC, ABL, AKT, HER, MAPK and SFK) versus the 228-peptide signatures of all other kinases (or all other kinases belonging to all other families) and all repeats, and then to select peptides associated with the most differential activities based on whether or not any of the 228-peptide-associated activity values passed a significance threshold of $P < 0.05$ for both an FDR-corrected t-test and a Wilcoxon rank-sum test. Importantly, this implies that: (1) the selected, most differential peptides can be associated with either low, high or 'average' phospho-catalytic activities specific to a kinase family as long as they significantly contrast with activities observed across all other kinases (following this principle, a peptide can be found as part of the differential signature of multiple kinase families owing to activity levels and significances that are specific to the differential signature of its given kinase

family versus all other kinases); and (2) the activities from the selected, most significantly differential peptides specific to a kinase family follow a trend that may vary from one individual kinase to another within that family (and/or between experimental readouts), and some individual kinases may also cluster away from the majority of other kinase family members (which would also underline the functional precision of combinatorial measurements provided by the HT-KAM strategy towards the systematic identification of specific enzymatic activity features unique to most kinases within a kinase family, yet remaining capable of functionally distinguishing some subfamily members). To confirm the validity of the differential peptide signature, the analysis was complemented using Monte Carlo cross-validation to further estimate how accurately our predictive model performed. Once this first part of the computational process was completed, the second step of this analysis was to extract all phospho-activity values established with the significantly differential peptides out of the 228-peptide profiles across all kinases and experiments, and then apply unsupervised hierarchical clustering to group peptides and kinases based on their functional relationships (see ranking trees to the top and left of each heat map shown in Fig. 1e and Supplementary Fig. 2g,h).

For the analysis in Fig. 1f and Supplementary Fig. 2i, the receiver operating characteristic (ROC) curves and AUC values for the specific subset of the most differential peptide combinations for each kinase or kinase family identified in Fig. 1e and Supplementary Fig. 2g,h were calculated using the m ethod developed in Fig. 1c and Supplementary Fig. 2a,b, but adapted to the exact set of peptides contributing to kinases' differential signatures. The same principle was used in Fig. 1d and Supplementary Fig. 2f to compute ROC curves and AUCs from the specific peptide phosphorylation profiles established with kinases' specific biological peptide subsets, generic CON[+] peptide subsets or random peptides.

For the analysis to generate heat maps in Fig. 4a,b, changes in the activity of kinases after V EM were measured using their respective subsets of biological peptides. Briefly, for each experimental run, the average value of ATP consumption across the 228 peptides and 14 data points from cell extract alone (that is, established from 14 peptide-free control wells per 384-well plate) was used for internal normalization. Each sample's kinase activity per peptide was then calculated as the difference in ATP consumption between individual peptide-derived readouts and the internal mean. Next, the peptide-specific activity values were averaged across repeats. Finally, the difference in phosphorylation activity per peptide between the VEM and control untreated (UNT) profiles was calculated across all 228 peptides. The results are represented as a series of kinase-focused heat maps using their particular subset of biological peptides. Each horizontal coloured bar within each heat map represents the differential activity in the presence of a biological peptide of the indicated kinase, ranging from blue to white to red, to respectively indicate lower to unchanged to higher activity after V EM treatment.

For the analysis generating the stacked bar plot in Fig. 4a,b, the relative cumulative index of kinases' activities was calculated as the average of the differential activity values (VEM - UN T) across all kinase-specific biological peptides, divided by the number of peptide sensors.

For the analysis leading to the heat map in Fig. 5a, the average value of ATP consumption in sample-containing wells measured across 228 peptides and 14 peptide-free controls was used for internal normalization for each experimental run. The activity per peptide was then calculated as the difference in ATP consumption between individual peptide-derived readouts and the internal mean. Next, peptide phosphorylation activity values were averaged across replicates. Finally, phospho-catalytic activity signatures measured across the 228-peptide sensors were subjected to unsupervised hierarchical clustering.

In Fig. 5b, the results are sorted by peptide class, then by highest to lowest range of phosphorylation activity per peptide. In Fig. 5c, the results are sorted by highest to lowest average phosphorylation activity per peptide, then subgrouped and counted to define which peptide class reports on the highest to lowest levels of phosphorylation activity. The technical reason to examine patterns of phosphorylation activity across peptide classes in Fig. 5b,c is that, for an assay to best distinguish the phosphorylation activities of different samples, it would be most appropriate to rely on phospho-sensing probes that capture the widest possible dynamic range of phosphorylation activities between cells, and/or provide the overall highest level of phosphorylation activity across cells. While asking this question, we also considered the possibility that the results of these two first variables may be different depending on the class of peptide used in the HT-KAM assay (that is, biological peptides, generic CON+ peptide probes or reference peptides).

In Fig. 7a, semisupervised hierarchical clustering was applied across the kinases (Euclidean distance) while maintaining the order of patients established in Fig. 6a.

To generate each kinase-focused subheat map of biological peptide phosphorylation activity profiles in Fig. 7b and Supplementary Fig. 2h, the levels of phosphorylation per peptide belonging to a kinase's biological peptide subset were averaged between different patients from specific groups.

In the bottom graph in Supplementary Fig. 1l, we calculated z-factor profiles because comparing the dynamic range with data variation of 'positive' versus 'negative' controls (that is, the z-factor or z') is a standard method in the field to evaluate the performance of an enzymatic assay. We used this method to: (1) assess the quality of individual assays included in HT-KAM experimental sets; and (2) evaluate how using different peptide probes impacts assay readout performance (since comparing z' outputs depending on peptides can be considered as a measure of the fitness of a probe in a kinase assay). The value of z' is calculated as z' = 1 – (3 × (positive s.d. + negative s.d.)/|positive mean – negative mean|), where negative values are ATP consumption values measured in the absence of any peptide (measured in the 14 peptide-free wells) and positive values are ATP consumption values measured in the presence of a peptide probe. Such a peptide probe is usually a commonly used generic CON[+] peptide, but can also correspond to other peptide probes included in our assay, such as either the best activity-reporting peptide among any other/non-advertised generic CON[+] for a tested kinase, or the best activity-reporting peptide among biological peptides (see graphs in Supplementary Fig. 1k,l).

In Supplementary Fig. 2e, AUCs of individual peptides (generic CON$^+$ or biological peptides) were calculated from repeated iterations of single-peptide sampling for kinases tested > 6 times (that is, ABL1, AKT1, EGFR, ERK2, p38a, HCK and SRC). This analysis compared all 228-peptide phospho-catalytic profiles across all 25 recombinant kinases and all experimental repeats using the principles described in Fig. 1c and Supplementary Fig. 2a,b, but applied to the particular case of $n = 1$. This method answers the question 'how good is an individual peptide at predicting the identity of a kinase?', and the results can be interpreted as: 'the higher a peptide's AUC for a particular kinase, the more this peptide (and this particular level of phosphorylation for this peptide) is good at discriminating this kinase from all other kinases'.

For the analysis in Supplementary Fig. 4a, each kinase was tested independent of all others, and we used 2 separate computational methods to compare the levels of ATP consumption per individual peptide with the pool of 63 reference peptides. In the first method, the average of 228 activity data points from all experimental repeats was used in a Kalmagorov-Smirnov test comparing each of 165 non-reference peptides (that is, 151 biological peptides and 14 generic CON$^+$ peptides) with the 63 reference peptides *(P* values with or without Benjamini-Hochberg correction controlling for the FD R). In parallel, the mean and s.d. of the 63 reference peptides was computed to then identify which peptides among the 165 non-reference peptides displayed activity signals greater than twofold s.d. from the mean (greater than the highest 2.5% of reference peptides). In the second method, instead of averaging the experimental replicates (as in the first method), they were used in either a linear additive model with Benjamini-Hochberg-corrected *P* values from each of the 165 non-reference peptides versus 63 reference peptides (threshold: BH.p.lam < 0.05), or an ANOVA model with Benjamini-Hochberg-corrected replicate error. The overlapping results of the statistical cut-offs of these two separate computational methods identify the most significantly and stringently selected high (and low) activities per peptide per kinase.

For the analysis in Supplementary Fig. 5d, every experimental phospho-signature was initially measured across all 228 peptides, and either in the presence or absence of the inhibitor (that is, each sample profile was normalized against the mean activity level measured across 228 peptides, then averaged across three independent replicates of each of the eight different conditions). The average activities measured in the presence of biological peptide targets of ABL1, ABL1^{T31SI}, LYNA or AKT1 were then measured.

In Supplementary Fig. 6d, data plotted on the *x* axis display the average of the activity differences across all biological peptides per kinase. Data plotted on the *y* axis use kinase activity levels calculated as: (1) the mean activity measured from the peptide subset that specifically differentiates the kinase in question from all other kinases, and that is associated with greater phosphorylation by the recombinant kinase in question, minus (2) the mean activity measured from the differential peptide subset specifically associated with lower phosphorylation by this kinase (that is, kinases' differential peptide sets identified in Fig. 1e,f and Supplementary Fig. 2g–i). For example, AKT1's increase activity is estimated at +82 based on its 20 biological peptide targets *(x* axis) and + 46 based on the difference between the average activity measured from AKT1's 21 most differentially high-activity peptides minus the average activity measured from AKT1's 6 most differentially low-

activity peptides (y axis). Such a method cross-validates the use of biological peptides as reporters of the activity of their kinases.

Other statistical and predictive methods used to compare sample groups and reproducibility between signatures included: unsupervised or semi-supervised hierarchical clustering using Euclidean distance, (absolute) correlation (centred or uncentred) and Ward linkage, or complete or average linkage to group phospho-activity signatures based on their similarities or differences; PCA; Student's *t*-test (FD R (Benjamini-Hochberg) corrected or not); Wilcoxon rank-sum test (FDR corrected or not; used either individually or as a dual-significance selection threshold *(P < 0.05))*; chi-squared *(X2)* test; and enrichment analysis using Fisher's one-sided test (EASE) to identify kinases whose peptides were most represented among sensor sets composed of a peptide signature.

Immunodetection and antibodies.

Cell lysates were resolved by sodium dodecyl sulfate gel electrophoresis (gels from Bio-Rad), followed by immunoblotting, as previously described[33,45] and following the manufacturer's instructions. Antibodies to detect ABL1 (catalogue number: 2862), ABL1 pY245 (catalogue number: 2861), AKT1/2/3 (catalogue number: 4691), AKT1/2 pS473 (catalogue number: 4060), AKT1/2 pT308 (catalogue number: 2965), EGFR (catalogue numbers 4267 and 3771), EGFR pY1068 (catalogue numbers 3777 and 2234), ERK1/2 (that is, MAPK1/ERK2/p44 and MAPK3/ERK1/p42; catalogue number: 4695), ERK1/2 pT202/Y204 (catalogue number: 4370), GSK3B (catalogue number: 9315), GSK3B pS9 (catalogue number: 9323), MAPK8/JNK1 (catalogue number: 3708), MAPK8/JNK1 pT183/pY185 (catalogue number: 9255), MAPK14/p38a (catalogue number: 8690), MAPK14/p38a pT180/pY182 (catalogue number: 9215), MEK1/2 (that is, MAP2K1 and MAP2K2; catalogue number: 4694), MEK1/2 pS217/221 (catalogue number: 9121), mTOR (catalogue number: 2972), mTOR pS2448 (catalogue number: 2971), MYC (catalogue number: 5605), PIM1 (catalogue number: 3247), PDPK1/PDK1 (catalogue number: 3062), PDPK1/PDK1 pS241 (catalogue number: 3438), PKN1/PRK1 pT774 and PKN2/PRK2 pT816 (catalogue number: 2611), PRKCA/PKCa (catalogue number: 2056), PRKCA/PKCa pT514 (catalogue number: 9379), RPS6KA1/p90RSK1 (catalogue number: 8408), RPS6KA1/p90RSK1 pT353 (catalogue number: 8753), RPS6KB1/p70S6K1 (catalogue number: 2708), RPS6KB1 pT389 (catalogue number: 9234), RPS6KB1/p70S6K1 pT421/pS424 (catalogue number: 9204), SGK1 (catalogue number: 3272) and SGK1 pS78 (catalogue number: 5599) were from Cell Signaling Technology. Antibodies to detect ERK1 (C –16), ERK2 (C-14), ERK1/2 pT202/pY204 (E-4), GAPDH (catalogue number: sc-32233) and HSP90 (catalogue number: sc-7947) were from SantaCruz. MYC pT58 (catalogue number: ab85380) was from Abcam. A mixture of ERK1 and ERK2 antibodies was used for the detection of total ERK[33]. Dilutions followed the manufacturers' instructions.

Technical notes.

Below, we provide technical considerations related to the assay, its utility and how we envision continuing to develop and improve its output.

We developed advanced computational methods and predictive statistical tools to demonstrate that the differential spectrum of low to medium to high phospho-catalytic activities measured across peptides makes it possible to use multipeptide libraries as modular systems to map many kinases with high sensitivity, specificity, differentiability and accuracy. This is the logical premise for using biological peptides of kinases as specific discriminators of kinases' respective identities and activities, and for using peptide libraries as a combinatorial system to simultaneously and directly measure the activities of many kinases at once in biological samples. Currently, no other enzymatic assay uses a multiplicity of (biological) peptide libraries as combinatorial sensors to concurrently identify and distinguish the catalytic activity levels of many kinases in cell or tissue extracts. All existing kinase enzyme activity assays are 'one-probe-to-many-kinases' assays that systematically rely on an individually used broad-spectrum consensus peptide with inherently limited specificity, and that cannot be used as a comprehensive, reliable, biological activity-testing system. As such, the strategy we developed (that is, a multipeptide-screening platform with computational/statistical analytical methods) is a fundamental conceptual and technical advance.

The 228 peptides we showcase in this study were selected based on the sentinel cancer-regulating role of the kinase/substrate targets they relate to, as defined in PhosphoAtlas30. Their selection was not based on the 25 recombinant kinases tested in Figs. 1–3. Instead, these 25 kinases were chosen as a means to validate the assay performance. We showed in cell lines and tumours that our assay identifies— and differentiates between—the altered, targetable activities of many other kinases than these 25 tested recombinant kinases (for example, M EKs, PDPK1, PIMs, RPS6KBs, GSK3, p38s, SGKs, p21-activated kinases (PAKs), PKNs, RPS6KAs, PKCs and JNKs; see Figs. 4, 5, 7 and 8 and Supplementary Figs. 6–8). We are currently developing and exploiting vastly expanded peptides libraries (including biological peptide sequences available from resources such as PhosphoAtlas; see Supplementary Fig. 1a,b) to explore, map and cover larger cancer signalling networks of kinase-dependent circuits.

To the full potential of the technical advances offered by the HT-KAM systems we showcase in this study, we currently concentrate on two main technological developments. First, we are expanding our peptide sensor library. Indeed, the results of our computational analyses of the differential spectrum of low-to-high phospho-catalytic activities measured across peptides directly predict that expanding the library beyond the current 228 peptides will enable the detection of many more kinases with even finer accuracy. Therefore, we are in the process of building a >600 peptide-screening platform, where biological peptide sensors are derived from hundreds of kinase-substrate nodes selected based on their critical function across malignancies and signalling pathways. Second, we are working towards computationally integrating HT-KAM-generated kinase activity signatures with the curated blueprint of kinase-substrate circuits available in PhosphoAtlas[30]. Indeed, progressing beyond a collection of siloed discrete data points, kinase activity profiles are of greatest value in their inherently integrated state to reflect the interconnected biological processes that wire tumours or cancer cells. Thus, we are in the process of developing novel computational methods to elucidate these higher functional orders, initially by projecting phospho-catalytic profiles onto PhosphoAtlas directional maps of protein-protein interaction

networks, and then by deriving pathways to identify and rank dominant signalling modules. This will address the current limitations of our technology, and effectively extend the functional coverage of the HT-KAM platform beyond its direct experimental readout and provide pathway-level coverage of phospho-signalling networks.

Concomitantly, and as part of the Cancer Cell Map Initiative consortium 5, we are also considering complementing our innovative experimental strategy and computational analyses described above with additional layers of molecular information, including ontology (for example Gene Ontology functions), as well as other proteomic scores (for example, mass spectrometry) or genomic data and large-scale drug responses. Our vision is that the integration of these non-overlapping/complementary layers of biological knowledge and high-throughput assay readouts will enable the mapping of signalling circuits with the breadth and detail necessary to reveal how dysfunctional, aberrant networks converge on vulnerable hotspots, which will substantially refine our understanding of the differential functional susceptibilities of tumours and be exploitable to overcome therapeutic resistance.

As an additional technical point, levels of phosphorylation measured with biological peptides available in the HT-KAM platform can be linked to both the functionality and phospho-protein states of the signalling circuits and adaptive response mechanisms that these biological peptides originate from (for example, EGFR, cell division cycle 25C[33], transforming growth factor beta receptor (TG FBR)[51] and m TOR in CRC (Supplementary Fig. 6e), and AKT, PIM RPS6KB, SFKs, Rapidly Accelerated Fibrosarcoma (RAF) and m TOR in melanoma[46,64–67] (Figs. 6d and 7a and Supplementary Fig. 7d–f)), with changes in biological peptide phosphorylation directly substantiated by western blots and internally validated with control-mutated biological peptide counterparts (CRC in Supplementary Fig. 6f–i and melanoma in Fig. 7d and Supplementary Fig. 7d). Noticeably, some of these biological peptides also match those that are 'paradoxically' more phosphorylated within kinases' phospho-signatures that otherwise exhibit low-activity profiles after VEM. For example, the subset of biological peptide sensors of ERK2 includes peptides related to the EG FR reactivation circuit (peptides derived from GAB1 T476/T312, GRB10 S150 and cRAF S289) and TG FBR pathway (SMAD2 S250; Fig. 4c, top left panel). The same applies to RPS6KA1 versus AKT1 (shared CREB1 S133 peptide), MAPK14 versus AKT1 (ATF2 T71) and MEK1 versus PDPK1 (cRAF T338), thus the phosphorylation status of some biological peptides can be associated with the early signs of activation of intrinsic resistance pathways (for example, reactivation of MEK/ERK signalling contributes to the insensitivity to RAF inhibition[34,67,68]), which outlines a valuable alternative potential utility for arrays of biological peptides such as those incorporated into the HT-KAM platform.

HT-KAM can be used as an exploratory/discovery platform to concurrently survey numerous kinases/kinase families and their activity levels, which is especially valuable in the case of diseases that cannot be defined by a single driver mutation or individual genetic dependencies (for example, BRAF[V600E] CRC or therapy-impervious melanoma). This advantage contrasts with short hairpin RNA (shRNA) or clustered regularly interspaced short palindromic repeats (CRISPR) genetic dropout screens that inevitably focus on finding a single, dominant genetic dependency, and necessarily require extrinsic interventions limited to cell culture models and that alter the dynamics of signalling circuits (details that

are particularly critical for understanding the adaptive rewiring of signalling circuits affecting drug responses). As such, the HT-KAM proteomic strategy can substantially refine the understanding of drug responses and help select drug candidates that target orthogonal modes of resistance with a high likelihood of circumventing adaptive responses, thus providing an innovative, rational approach to the prioritization and design of novel treatment opportunities capable of inducing maximum lethal effect on tumours. The fact that our platform is focused on a subset of actionable targets and identifies wild-type and mutated targets significantly increases its translational impact.

Step-by-step protocols.

The step-by-step biochemical assay protocol and the step-by-step data/computational analysis protocol developed in this study can be found at Nature's Protocol Exchange[69,70].

Reporting Summary.

Further information on research design is available in the Nature Research Reporting Summary linked to this article.

Data availability

The human melanoma data were derived from the TCGA Research Network (http:// cancergenome.nih.gov/). The RNA-Seq dataset derived from this resource that supports the findings of this study is available in the TCGA, Skin Cutaneous Melanoma repository accessed and analysed online using cBioPortal (http://www.cbioportal.org). RNA-Seq data that support the findings of this study have been deposited in the Gene Expression Omnibus under accession code G SE129127. Source data for Figs. 1, 2, 3a, 4a, b, 5a, 6a and 7d and Supplementary Figs. 1e–h, 1k,l, 2–5, 6 d–f and 7c have been provided as Supplementary Table 26. All other data supporting the findings of this study are available from the corresponding author on reasonable request.

Supplementary Material

Refer to Web version on PubMed Central for supplementary material.

Acknowledgements

## References

1. Petricoin EF, Zoon KC, Kohn EC, Barrett JC & Liotta LA Clinical proteomics: translating benchside promise into bedside reality. Nat. Rev. Drug Discov 1, 683–695 (2002). [PubMed: 12209149]

2. Blume-Jensen P & Hunter T Oncogenic kinase signalling. Nature 411, 355–365 (2001). [PubMed: 11357143]

3. Fleuren ED, Zhang L, Wu J & Daly RJ The kinome 'at large' in cancer. Nat. Rev. C ancer 16, 83–98 (2016).

4. Johnson SA & Hunter T Kinomics: methods for deciphering the kinome. Nat. Methods 2, 17–25 (2005). [PubMed: 15789031]

5. Krogan NJ, Lippman S, Agard DA, Ashworth A & Ideker T The Cancer Cell Map Initiative: defining the hallmark networks of cancer. Mol. Cell 58, 690–698 (2015). [PubMed: 26000852]

6. Hoadley KA et al. Multiplatform analysis of 12 cancer types reveals molecular classification within and across tissues of origin. Cell 158, 929–944 (2014). [PubMed: 25109877]

7. Akbani R et al. A pan-cancer proteomic perspective on The Cancer Genome Atlas. Nat. Commun 5, 3887 (2014). [PubMed: 24871328]

8. Chandarlapaty S et al. AKT inhibition relieves feedback suppression of receptor tyrosine kinase expression and activity. Cancer Cell 19, 58–71 (2011). [PubMed: 21215704]

9. Coppe JP et al. Senescence-associated secretory phenotypes reveal cell-nonautonomous functions of oncogenic RAS and the p53 tumor suppressor. PLoS Biol. 6, 2853–2868 (2008). [PubMed: 19053174]

10. Huttlin EL et al. The BioPlex Network: a systematic exploration of the human interactome. Cell 162, 425–440 (2015). [PubMed: 26186194]

11. Rikova K et al. Global survey of phosphotyrosine signaling identifies oncogenic kinases in lung cancer. Cell 131, 1190–1203 (2007). [PubMed: 18083107]

12. Zhang B et al. Proteogenomic characterization of human colon and rectal cancer. Nature 513, 382–387 (2014). [PubMed: 25043054]

13. Uhlen M. et al. Proteomics. Tissue-based map of the human proteome. Science 347, 1260419 (2015). [PubMed: 25613900]

14. Drake JM. et al. Phosphoproteome integration reveals patient-specific networks in prostate. Cancer Cell 166, 1041–1054 (2016).

15. Sharma K et al. Ultradeep human phosphoproteome reveals a distinct regulatory nature of Tyr and Ser/Thr-based signaling. Cell Rep. 8, 1583–1594 (2014). [PubMed: 25159151]

16. Duncan JS et al. Dynamic reprogramming of the kinome in response to targeted M EK inhibition in triple-negative breast cancer. Cell 149, 307–321 (2012). [PubMed: 22500798]

17. Sos ML et al. Oncogene m im icry as a mechanism of primary resistance to BRAF inhibitors. Cell Rep. 8, 1037–1048 (2014). [PubMed: 25127139]

18. Bantscheff M. et al. Quantitative chemical proteomics reveals mechanisms of action of clinical ABL kinase inhibitors. Nat. Biotechnol 25, 1035–1044 (2007). [PubMed: 17721511]

19. Daub H et al. Kinase-selective enrichment enables quantitative phosphoproteomics of the kinome across the cell cycle. Mol. Cell 31, 438–448 (2008). [PubMed: 18691976]

20. Kubota K et al. Sensitive multiplexed analysis of kinase activities and activity-based kinase identification. Nat. Biotechnol 27, 933–940 (2009). [PubMed: 19801977]

21. Nomura DK, Dix MM & Cravatt BF. Activity-based protein profiling for biochemical pathway discovery in cancer. Nat. Rev. Cancer 10, 630–638 (2010). [PubMed: 20703252]

22. Ren W, Damayanti NP, Wang X & Irudayaraj JM. Kinase phosphorylation monitoring with i-m otif DNA cross-linked SERS probes. Chem. Commun. (C am b.) 52, 410–413 (2016).

23. Anastassiadis T, Deacon SW, Devarajan K, Ma H & Peterson JR Comprehensive assay of kinase catalytic activity reveals features of kinase inhibitor selectivity. Nat. Biotechnol 29, 1039–1045 (2011). [PubMed: 22037377]

24. Houseman BT, Huh JH, Kron SJ & Mrksich M. Peptide chips for the quantitative evaluation of protein kinase activity. Nat. Biotechnol 20, 270–274 (2002). [PubMed: 11875428]

25. Karaman MW et al. A quantitative analysis of kinase inhibitor selectivity. Nat. Biotechnol 26, 127–132 (2008). [PubMed: 18183025]

26. Fang C et al. Integrated microfluidic and imaging platform for a kinase activity radioassay to analyze minute patient cancer samples. Cancer Res. 70, 8299–8308 (2010). [PubMed: 20837665]

27. Li X. et al. The reverse in-gel kinase assay to profile physiological kinase substrates. Nat. Methods 4, 957–962 (2007). [PubMed: 17952089]

28. Wu J, Barbero R, Vajjhala S & O 'Connor SD Real-time analysis of enzyme kinetics via micro parallel liquid chromatography. Assay Drug Dev. Technol 4, 653–660 (2006). [PubMed: 17199503]

29. Sanz A et al. Analysis of Jak2 catalytic function by peptide microarrays: the role of the JH2 domain and V 617F mutation. PLoS ONE 6, e18522 (2011). [PubMed: 21533163]

30. Olow A et al. An atlas of the human kinome reveals the mutational landscape underlying dysregulated phosphorylation cascades in cancer. Cancer Res. 76, 1733–1745 (2016). [PubMed: 26921330]

31. Hornbeck PV et al. PhosphoSitePlus, 2014: mutations, PTM s and recalibrations. Nucleic Acids Res 43, D 512–D 520 (2015).

32. Yang X et al. Widespread expansion of protein interaction capabilities by alternative splicing. Cell 164, 805–817 (2016). [PubMed: 26871637]

33. Prahallad A et al. Unresponsiveness of colon cancer to BRA F(V600E) inhibition through feedback activation of EGFR. Nature 483, 100–103 (2012). [PubMed: 22281684]

34. Corcoran RB et al. EGFR-mediated re-activation of MAPK signaling contributes to insensitivity of BRAF mutant colorectal cancers to RAF inhibition with vemurafenib. Cancer Discov. 2, 227–235 (2012). [PubMed: 22448344]

35. Yang H et al. Antitumor activity of BRAF inhibitor vemurafenib in preclinical models of BRAF-mutant colorectal cancer. Cancer Res. 72, 779–789 (2012). [PubMed: 22180495]

36. Van Geel RM., Beijnen JH, Bernards R. & Schellens JH. Treatment individualization in colorectal cancer. Curr. Colorectal Cancer Rep 11, 335–344 (2015). [PubMed: 26617477]

37. Corcoran RB et al. Combined BRAF, EGFR, and M EK inhibition in patients with BRA F(V600E)-m utant colorectal cancer. Cancer Discov. 8, 428–443 (2018). [PubMed: 29431699]

38. Ursem C, Atreya CE & Van Loon K Emerging treatment options for BRAF-m utant colorectal cancer. Gastrointest. Cancer 8, 13–23 (2018). [PubMed: 29628780]

39. Bernards R A missing link in genotype-directed cancer therapy. Cell 151, 465–468 (2012). [PubMed: 23101617]

40. Flaherty KT et al. Combined BRAF and M EK inhibition in melanoma with BRAF V 600 mutations. N. Eng. J. M ed 367, 1694–1703 (2012).

41. Larkin J et al. Combined vemurafenib and cobimetinib in BRAF-mutated melanoma. N. Eng. J. M ed 371, 1867–1876 (2014).

42. Van Allen EM. et al. The genetic landscape of clinical resistance to RAF inhibition in metastatic melanoma. Cancer Discov. 4, 94–109 (2014). [PubMed: 24265153]

43. Wagle N et al. MAP kinase pathway alterations in BRAF-mutant melanoma patients with acquired resistance to combined RAF/MEK inhibition. Cancer Discov. 4, 61–68 (2014). [PubMed: 24265154]

44. Cancer Genome Atlas Network. Genom ic classification of cutaneous melanoma. Cell 161, 1681–1696 (2015). [PubMed: 26091043]

45. Kemper K et al. BRA F(V600E) kinase domain duplication identified in therapy-refractory melanoma patient-derived xenografts. Cell Rep. 16, 263–277 (2016). [PubMed: 27320919]

46. Johannessen CM et al. COT drives resistance to RAF inhibition through MAP kinase pathway reactivation. Nature 468, 968–972 (2010). [PubMed: 21107320]

47. Janne PA, Gray N & Settleman J Factors underlying sensitivity of cancers to small-molecule kinase inhibitors. Nat. Rev. Drug Discov 8, 709–723 (2009). [PubMed: 19629074]

48. Ruiz-Saenz A & Moasser MM. Targeting HER2 by combination therapies. J. Clin. Oncol 36, 808–811 (2018). [PubMed: 29381433]

49. Cohen RL & Settleman J From cancer genomics to precision oncology—tissue's still an issue. Cell 157, 1509–1514 (2014). [PubMed: 24949964]

50. Holohan C, Van Schaeybroeck S, Longley DB & Johnston PG Cancer drug resistance: an evolving paradigm. Nat. Rev. Cancer 13, 714–726 (2013). [PubMed: 24060863]

51. Brunen D et al. TGF-β: an emerging player in drug resistance. Cell Cycle 12, 2960–2968 (2013). [PubMed: 23974105]

52. Garnett MJ. et al. Systematic identification of genomic markers of drug sensitivity in cancer cells. Nature 483, 570–575 (2012). [PubMed: 22460902]

53. Kemper K et al. Intra- and inter-tum or heterogeneity in a vemurafenib-resistant melanoma patient and derived xenografts. EMBO Mol. Med 7, 1104–1118 (2015). [PubMed: 26105199]

54. Breitinger H-G. Drug Synergy—Mechanisms and Methods of Analysis (InTech, 2012).

55. Chou TC & Talalay P Quantitative analysis of dose-effect relationships: the combined effects of multiple drugs or enzyme inhibitors. Adv. Enzyme Regul 22, 27–55 (1984). [PubMed: 6382953]

56. Berenbaum MC. Synergy, additivism and antagonism in immunosuppression. A critical review. Clin. Exp. Immunol 28, 1–18 (1977). [PubMed: 324671]

57. Foucquier J & Guedj M. Analysis of drug combinations: current methodological landscape. Pharmacol. Res. Perspect 3, e00149 (2015). [PubMed: 26171228]

58. Berenbaum MC. What is synergy? Pharmacol. Rev 41, 93–141 (1989). [PubMed: 2692037]

59. Bliss WL Early man in western and northwestern Canada. Science 89, 365–366 (1939).

60. Arao T et al. Small in-fram e deletion in the epidermal growth factor receptor as a target for ZD 6474. Cancer Res. 64, 9101–9104 (2004). [PubMed: 15604279]

61. Yang W et al. Genomics of Drug Sensitivity in Cancer (G DSC): a resource for therapeutic biomarker discovery in cancer cells. Nucleic Acids Res. 41,D955–D961 (2013). [PubMed: 23180760]

62. Daemen A et al. Modeling precision treatment of breast cancer. Genome Biol. 14, R110 (2013). [PubMed: 24176112]

63. Moasser M, Srethapakdi M., Sachar KS, Kraker AJ & Rosen N. Inhibition of Src kinases by a selective tyrosine kinase inhibitor causes mitotic arrest. Cancer Res. 59, 6145–6152 (1999). [PubMed: 10626805]

64. Nazarian R et al. Melanomas acquire resistance to B-RA F(V 600E) inhibition by RTK or N-RAS upregulation. Nature 468, 973–977 (2010). [PubMed: 21107323]

65. Sun C et al. Reversible and adaptive resistance to BRA F(V 600E) inhibition in melanoma. Nature 508, 118–122 (2014). [PubMed: 24670642]

66. Girotti MR et al. Paradox-breaking RAF inhibitors that also target SRC are effective in drug-resistant BRAF mutant melanoma. Cancer Cell 27, 85–96 (2015). [PubMed: 25500121]

67. Poulikakos PI, Zhang C, Bollag G, Shokat KM. & Rosen N RAF inhibitors transactivate RAF dimers and ERK signalling in cells with wild-type BRAF. Nature 464, 427–430 (2010). [PubMed: 20179705]

68. Ahronian LG et al. Clinical acquired resistance to RAF inhibitor combinations in BRAF-mutant colorectal cancer through M APK pathway alterations. Cancer Discov. 5, 358–367 (2015). [PubMed: 25673644]

69. Mori M., Pan B. & Coppe JP. High-throughput kinase activity mapping (HT-KAM) system: biochemical assay. Nat. Protoc. Exch 10.1038/protex.2019.029 (2019).

70. Yau C, Wolf DM. & Coppe JP High-throughput kinase activity mapping (HT-KAM) system: analysis of phospho-catalytic profiles. Nat. Protoc. Exch 10.1038/protex.2019.030 (2019).

Coppé et al.

Page 30
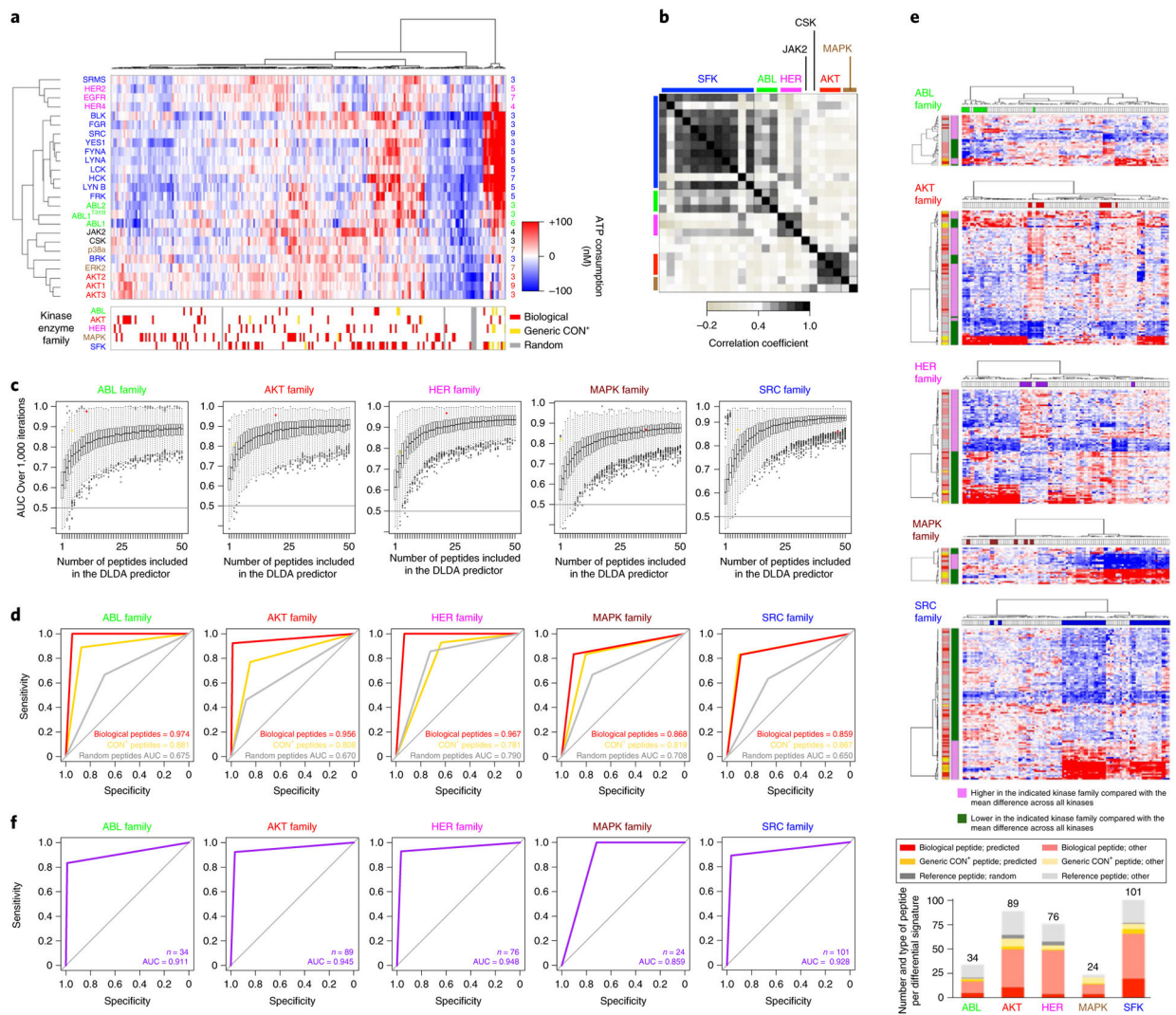
Fig. 1 |. Arrays of peptides function as combinatorial sensors to identify, differentiate and measure the phosphorylation activity of kinases.

a, Unsupervised hierarchical clustering of the phospho-catalytic activity signatures of 25 recombinant purified kinases monitored across 228 peptides. For each experimental run, the average value of ATP consumption across 228 peptides was used for internal normalization. The kinase activity per peptide was then calculated as the difference in ATP consumption between individual peptide-derived values and the internal mean (Supplementary Table 26). Peptide-specific activity values were then averaged across independent repeats to establish the activity signature of each kinase across all peptide sensors. The numbers of independent experimental repeats are shown to the right. The peptide color key defining peptides' category and relationship to kinases is indicated at the bottom right (red/gold/grey). The phospho-catalytic activity scale (blue-to-white-to-red) is in nM of ATP consumption, where 0 (white) is the mean activity value measured across 228 peptides for a given kinase. **b**, Pearson correlation heat map highlighting the functional relationships of kinase enzymes based on their 228-peptide phosphorylation signatures. **c**, AUC profiles obtained for an increasing number of randomized sampling combinations of peptide sensors to identify a

kinase family. AUC values (yaxis) reflect the performance of the assay for predicting the identity of a kinase family by comparing all of its kinases' 228-peptide phospho-signatures versus the 228-peptide phospho-signatures of all other kinases, when relying on one or multiple peptide sensors (xaxis; random peptide sampling of combinations of up to 50 peptides out of 228 using DLDA class predictors). Box edges represent the 25th and 75th percentiles, the central line is the median, and whiskers represent the 25th and 75th percentiles + 1.5x the IQR. Points show outlier data falling outside the range. **d**, For each kinase family, receiver operating characteristic (ROC) curves and AUC values (numbers within each plot) were computed from kinases' phospho-catalytic activity profiles measured with either their individual biological peptide subset (red), their generic CON+ peptide subset (gold) or random peptides (grey). **e,f**, Identification of combinatorial peptide sets that best differentiate the phospho-catalytic activities of kinase families. All 228-peptide activity profiles from a given family were compared with the profiles of all other kinases. Peptides associated with differential activity values (up or down) passing a significant $P < 0.05$ threshold for both an FDR-corrected f-test and Wilcoxon rank-sum test were selected. Activity heat maps in e show the unsupervised hierarchical clustering of the phospho-catalytic activity profiles established with the differential peptide subsets (y-axis) predictive of the identity of a kinase family in comparison to the activity profiles of all other kinases (x axis). Heatmaps show that distinct subsets of peptides can be systematically identified as functional predictors of the differential activity signature of each kinase family. In the bottom graph, biological or generic CON[+] peptides composing the differential signatures were classified as 'predicted' or not ('other'), where 'predicted' defines a peptide previously identified in the literature as a target of a given kinase. The reference peptides were categorized as either random or not random ('other', that is mutated biological or generic CON[+] peptides).This peptide color key is also indicated on the far left of the veritcal axis of the heatmaps. ROC curves in **f** were calculated from the differential peptide sets per kinase family signature identified in panel **e**. Numbers of peptides and AUC values are shown in each plot.
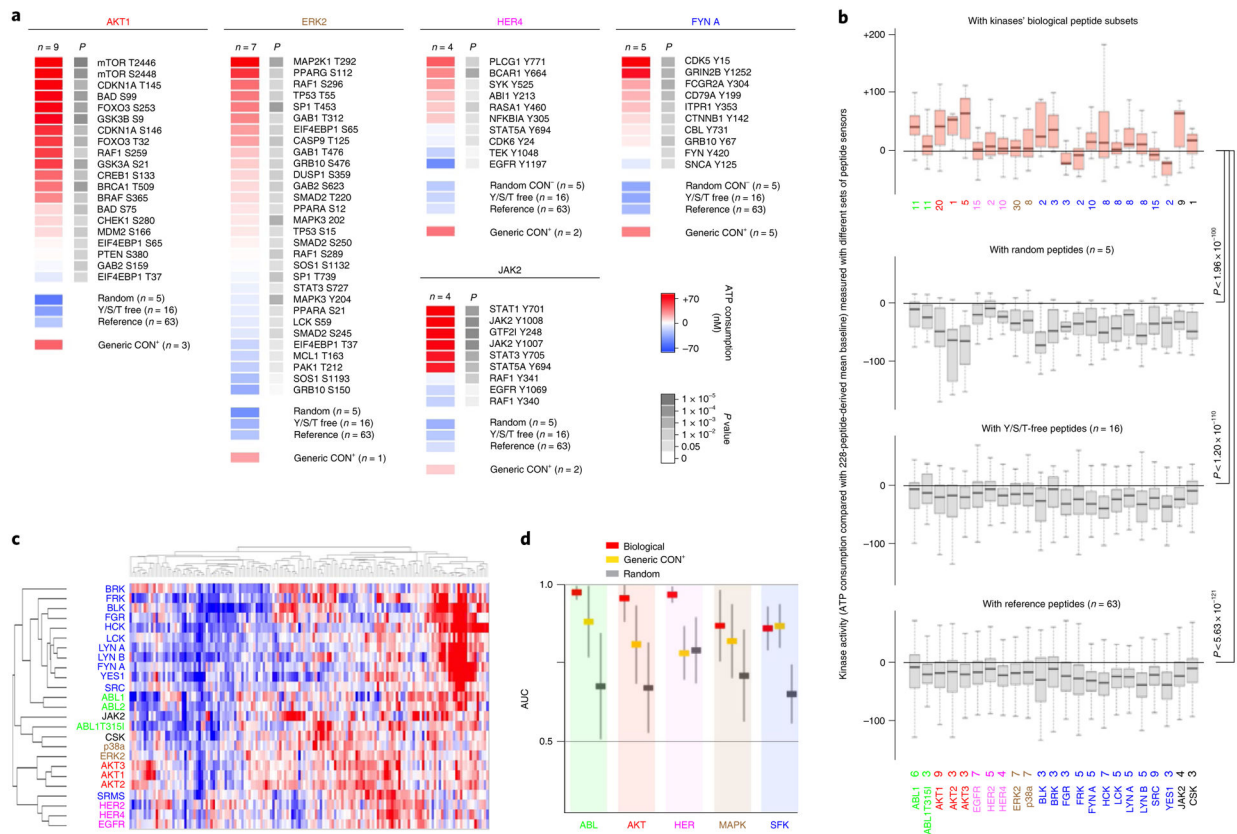
Fig. 2 |. The biological peptide targets of kinases are effective sensors of kinases' phospho-catalytic activities.

a, Examples of peptide phosphorylation activity profiles (extracted from Fig. 1a) measured with kinases' biological peptides. Biological peptides, named by their substrate protein and phosphotarget site of origin, are indicated to the right of each panel, and are sorted top-to-bottom from highest-to-lowest activity per kinase. Average activities measured with control peptide sets (random, Y/S/T free, reference and generic CON⁺) are shown below for comparison. The grey colour scale represents the significance of a comparison between the activities from biological peptides versus average random peptides (two-sided Student's f-test, Benjamini-Hochberg corrected and paired across experiments). **b**, Comparison between the levels of kinases' activities measured in the presence of their biological peptide subsets versus random, Y/S/T-free or all reference peptides. Central bars represent medians, box edges represent the first and third interquartile ranges, and whiskers represent the minimum and maximum values. Significance values, as determined by two-sided Student's f-test, are reported to the right. Numbers below the top plot represent the numbers of biological peptides per kinase. Numbers below the bottom plot represent the numbers of independent experimental repeats per kinase. **c**, Unsupervised hierarchical clustering of kinases' activity signatures using biological peptides. Only activities measured with the 151 biological peptides out of the 228-peptide profiles in Fig. 1a were used for ranking. **d**, AUC forest plot comparing the specificity/sensitivity of activity profiles established with different peptide sets. Data points and error bars represent means ±s.d.
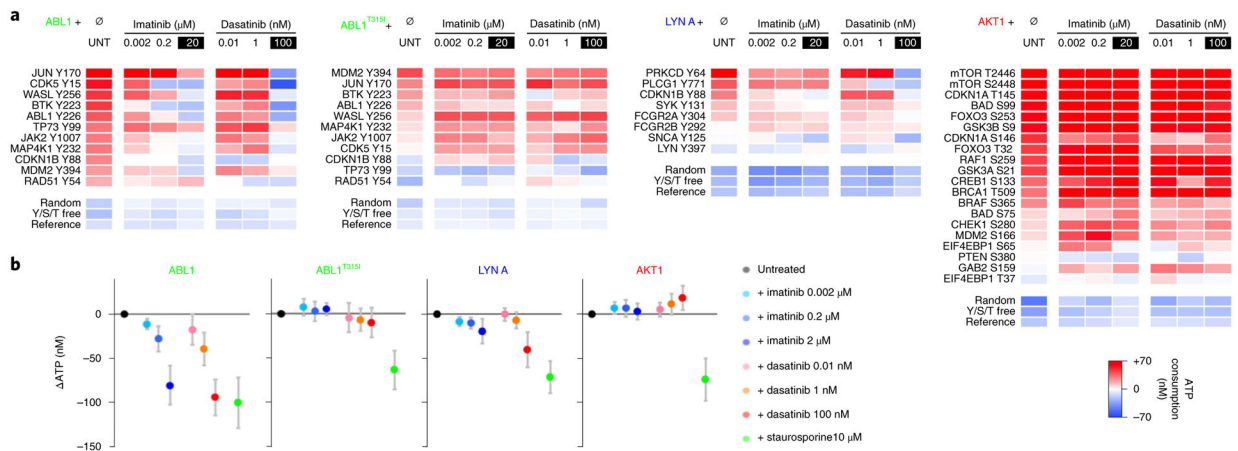
Fig. 3 |. Measuring the effects of kinase inhibitors using kinases' biological peptide subsets as functional sensors of drug response and sensitivity.

a, Effects of kinase-targeting drugs on the activity of kinases using kinases' respective subsets of biological peptides as functional sensors of changes in phospho-catalytic activity (Supplementary Table 26). The chosen concentrations of imatinib and dasatinib correspond to ABL1's 0.01, 1x and 100x IC50 concentrations. Imatinib and dasatinib are anticipated to have less effect on LYNA (respective IC_{50}s: 100 μM and 9 nM), and minimal or no effect on ABL1[T315I] or AKT1. '**0**' means control untreated (UNT). The biological peptides corresponding to the indicated kinase and included in the 228-peptide sensor library are named by their substrate protein and phosphotarget site of origin (indicated to the left of each panel) and are sorted top-to-bottom from highest-to-lowest activity per kinase measured in control untreated assay condition. Numbers of peptides in the control category were as follows: random, *n* = 5; Y/S/T free, n = 16; reference, *n* = 63. **b**, Shifts in activities comparing untreated versus inhibitor-treated ABL1, ABL1[T31a], LYNA and AKT1 kinases, calculated as averages of the differential kinase activity changes measured across their biological peptides (see Supplementary Fig. 5a). Staurosporine serves as a control for the general shutdown of kinase activity. Data points and error bars represent means ±s.d.
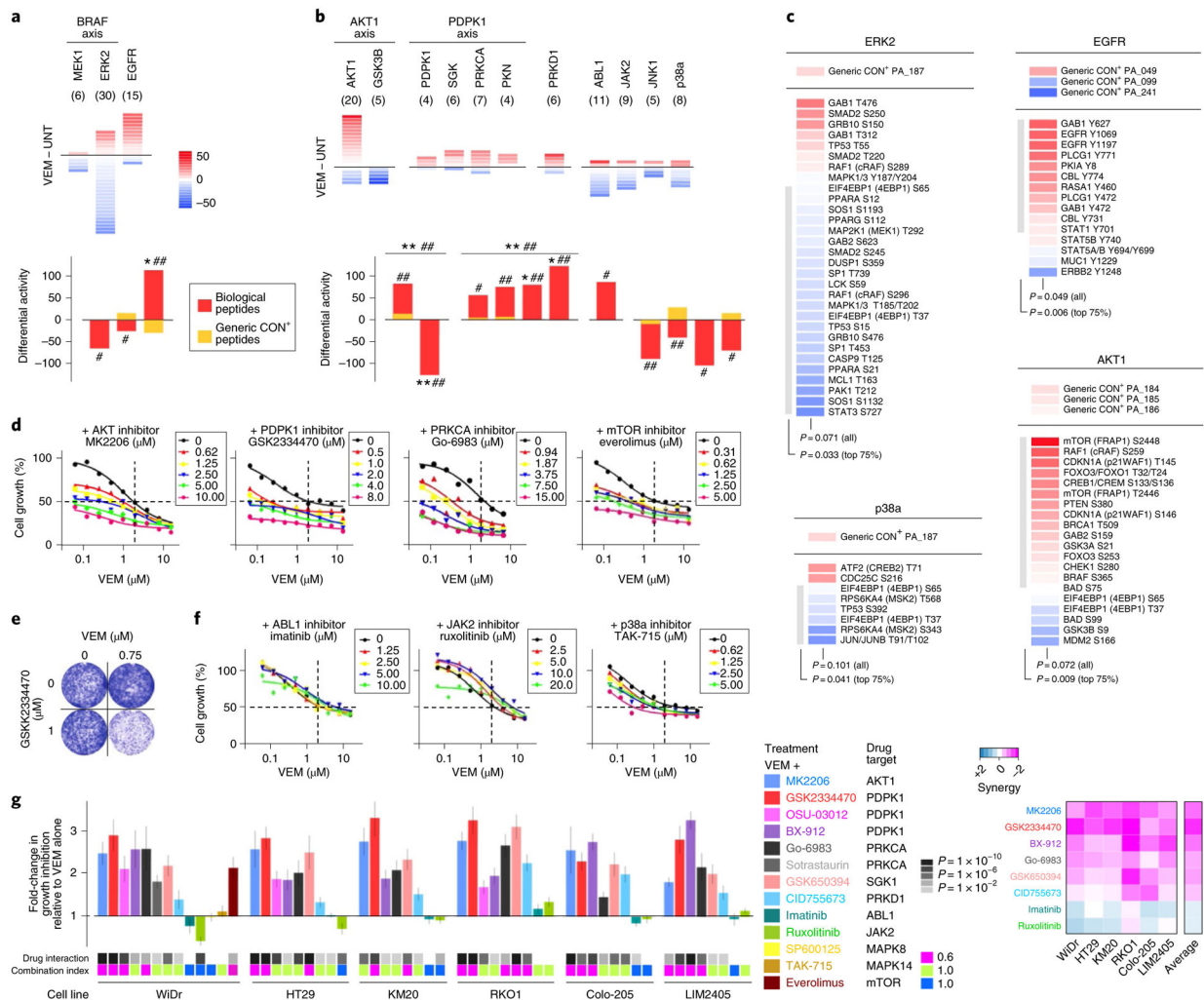
Fig. 4 |. Mapping the phospho-catalytic signatures of BRAF^V600E therapy-resistant CRC cells identifies druggable kinase vulnerabilities for combinatorial therapy.

a, Changes in the activity of kinase enzymes induced by BRAF^V600E-targeting therapy in WiDr cells. Heat maps (top) show changes in kinases' activity using their respective subsets of biological peptides. Each horizontal coloured bar represents the differential activity measured in the presence of a kinase's biological peptide (Supplementary Table 26), with higher (or unchanged or lower) biological peptide phosphorylation after VEM indicated in red (or white or blue) (in nM of differential ATP consumption between VEM and UNT). Numbers of biological peptide sensors per kinase are shown in brackets. Bar plots (bottom) show a relative cumulative index of kinases' activities (in nM ATP) as an indicator of their functional change in response to VEM (red versus gold bars; activities were derived from kinases' biological versus CON⁺ peptides). Significance was measured using a pairwise two-sided Student's f-test comparing VEM and UNT across all runs (*/#: P<0.05; **/##: P<0.01), including either all biological peptides (*/**) or 75% of biological peptides that follow the main activity trend (#/##), to elude cross-reaction effects from parallel feedback loops such as AKT or EGFR, as illustrated with ERK2's biological peptides that paradoxically display higher activity (few red bars at the top of the ERK2 heat map) but

relate to proteins involved in resistance mechanisms, including the EGFR and TGFBR pathways[33–35–51]. **b**, Identification of other kinases mediating the VEM response. PRKD1, protein kinase D1. **c**, Examples of kinases' differential activity profiles measured with their CON$^+$ peptides (top) or biological peptide subsets (bottom). A grey side bar outlines the top 75% of biological peptides that follow the main activity trend. d, Response of WiDr to combinatorial drug treatments in three-day survival assays. Everolimus serves as a positive control for circumventing intrinsic VEM resistance ($n = 3$). e, WiDr colony formation assessing the cells' sensitivity to BRAF^{V600E} + PDPK1 inhibition ($n = 2$). **f**, Response of WiDr cells to inhibitors targeting kinases whose phospho-catalytic activities are not upregulated after VEM. **g**, Sensitivity of different BRAF^{V600E} CRC cell lines to combinations of VEM plus a second drug ($n > 2$). Bar plots display mean±s.d. fold-changes in VEM sensitivity at concentrations <GI$_{50}$ of drug alone for each cell line. P values for drug interactions were calculated by two-way ANOVA (grey scale), while combination indices were calculated using the Loewe model (pink-green-blue scale). The heat map to the far right shows the combination index derived from Bliss model analysis, and averaged from experimentally measured combination indices at GI$_{50}$, $2 \times$ GI$_{50}$ and $0.5 \times$ GI$_{50}$ concentrations of each drug. The drug responses serve as validation of the kinase activity signatures uncovered by HT-KAM, and illustrate how such a strategy can help in the selection of drug candidates to restore therapeutic sensitivity.
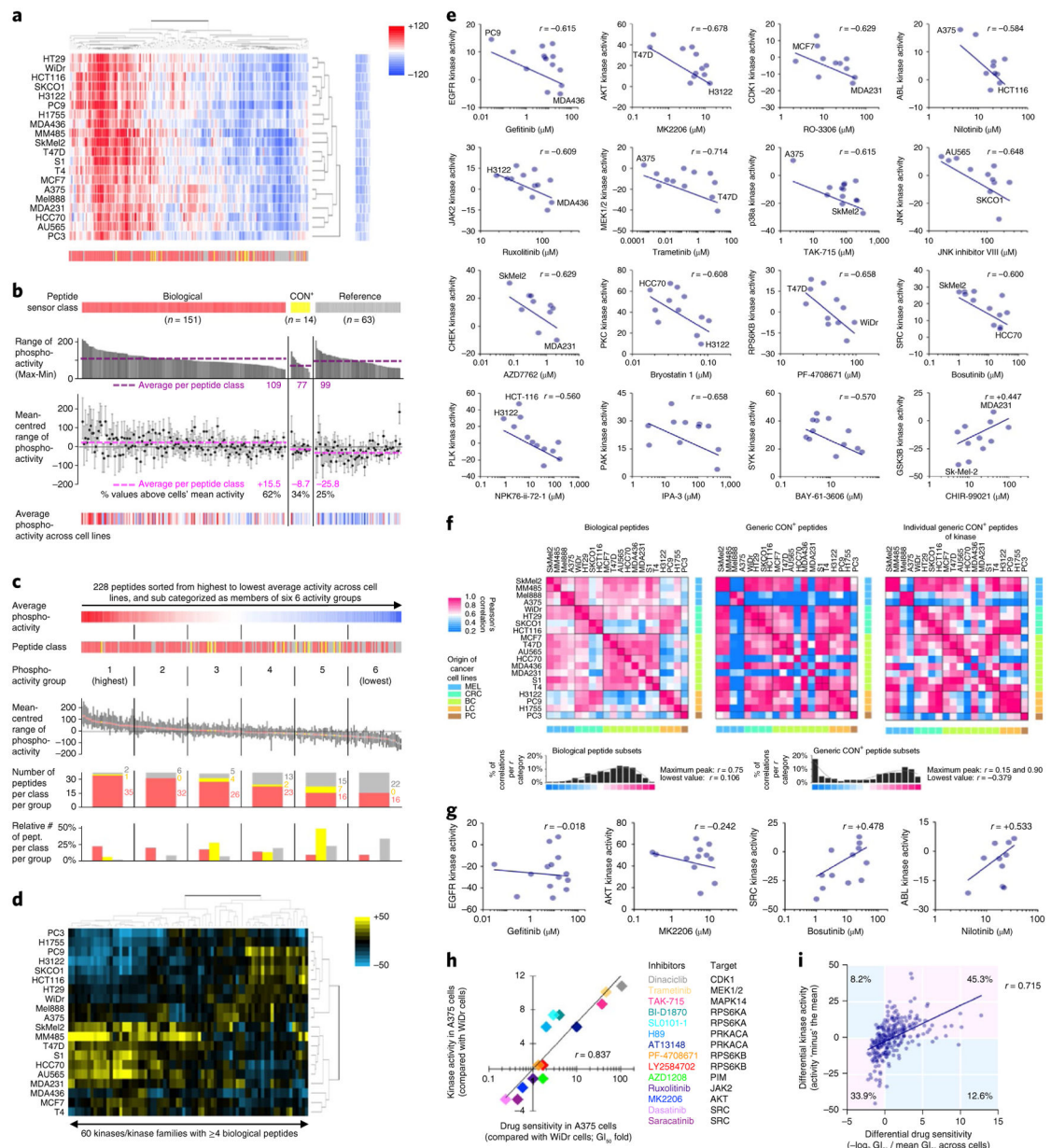
Fig. 5 |. Cancer cells' phospho-catalytic signatures reveal a wide spectrum of kinase activities indicative of differential dependencies and vulnerabilities to kinase-targeting agents.

a, Unsupervised hierarchical clustering of the peptide phosphorylation activity signatures of 20 cancer cell lines. For each experimental run, the average value of ATP consumption in sample-containing wells measured across 228 peptides and 14 peptide-free controls was used for internal normalization (Supplementary Table 26). The activity per peptide was then calculated as the difference in ATP consumption between individual peptide-derived readouts and the internal mean. Phospho-catalytic activities are colour-coded based on the relative level of activity measured in the presence of each peptide for each cell line (blue, low activity; white, intermediate or mean activity; red, high activity; in nM of ATP consumption). The bottom red/ gold/ grey streak indicates the category of biological peptides / generic CON+ peptides / reference peptides out of the 228 peptides. The heatmap

on the right represents cells' activity measured in the 14 control, peptide-free wells. **b,c**, Peptide phosphorylation activity patterns across cancer cells based on the range of activity per peptide, average level of phosphorylation intensity per peptide, and peptide class. In b, peptides are first sorted by peptide category and then range of peptide-phosphorylation activity per peptide. In the plots of mean-centred ranges of phospho-activity, the data points represent the mean, while the error bars represent maximum and minimum values. In c, peptides are first sorted by average peptide-phosphorylation activity per peptide. **d**, Unsupervised hierarchical clustering of the kinase activity signatures of 20 cancer cell lines. For each cell line, kinase activities were calculated as the average of the phosphorylation activities measured in presence of kinases' respective biological peptide subsets (deconvoluted from the peptide phosphorylation profiles in **a**). Profiles were then mean-centred across cell lines. Profiles highlight the heterogeneity of kinases' activities across cancer cells. **e**, Comparison of cancer cells' drug sensitivity (x axis; GI50 concentration per drug per cell line) versus the kinase activity (y axis) derived from the biological peptide subsets in **d**. Each data point represents a cell line. Pearson correlation coefficients (r) are included within each plot. CHEK, checkpoint kinase; SYK, spleen tyrosine kinase. **f**, Pearson correlation heat maps highlighting the functional relationship between cancer cells based on their kinase activity signatures established from kinases' subsets of biological peptides (left), versus kinases' subsets of generic CON$^+$ peptides (middle), or individual generic CON$^+$ peptides of kinases (right). Cells are arranged by tumour origin (BC, breast cancer; LC, lung cancer; MEL, melanoma; PC, prostate cancer). **g**, Comparison of cancer cells' drug sensitivity versus the kinase activity derived from the kinases' subsets of generic CON$^+$ peptides. Each data point represents a cell line. Pearson correlation coefficients (*r*) are included within each plot. **h**, Pearson correlation between kinase activity and drug sensitivity in A375 (melanoma) versus WiDr (CRC) BRAF^{V600E} cells *(n = 2* per data point). **i**, Pearson correlation between kinase activity and drug sensitivity across all results (373 data points derived from 35 drug treatments targeting 23 kinases are plotted).
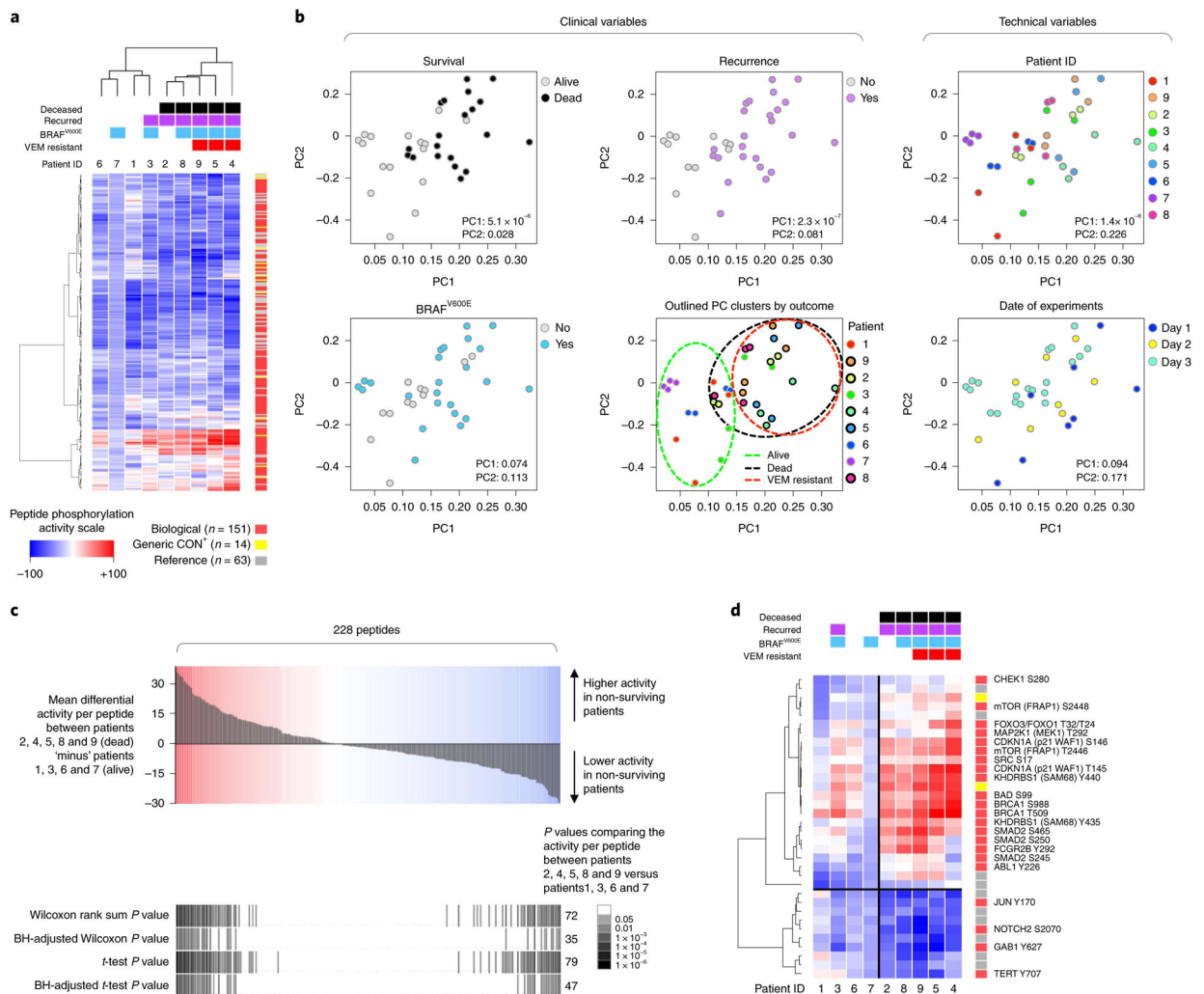
Fig. 6 |. Mapping the peptide phosphorylation signatures of melanoma tumours is predictive of patients' outcome and BRAF therapy resistance.

a, Peptide phosphorylation signatures of nine patient tumours (Supplementary Table 26). Data analysis followed the same steps as for cell extracts (n = 4 per sample). HT-KAM-generated profiles were clustered using Euclidean distance and ward linkage. Retrospective information on survival outcome, recurrence and treatment resistance is indicated above the heat map, along with BRAFV600E mutational status (see Supplementary Table 18). Colour bar values are in nM ATP. **b**, PCA investigating the potential association between variables of interest and principal components (PCs) defining the phosphorylation signatures of tumour samples (linear regression; overall fit of univariate model PC *i* for variable j). Graphs display the results for a clinical or technical variable and its significance. F-statistic P values are presented in the bottom right of each plot. Each data point corresponds to one experimental run for one tumour sample (9 patients × 4 independent experimental replicates for each patient tumour = 36 dots per graph). **c,d**, Methods to find peptides that qualify as the best predictors of patients' outcome. **c**, Waterfall plot showing the differential activity profile (y axis) across 228-peptide sensors (x axis), comparing alive versus deceased patient groups. Significance values are provided underneath, along with the numbers of peptides

displaying a P value of < 0.05 (to the right). **d**, Peptides were selected from **c** when phosphorylation activities concurrently passed both the FDR-adjusted two-sided f-test and Wilcoxon rank-sum test at P< 0.05, and subjected to semi-supervised clustering to compare the differential phosphorylation activity in patients who were alive and those who were not. The rigorous dual-significance threshold selection identified 34 peptides as the most significantly differentially phosphorylated peptides associated with poor outcome, as shown across individual patients. Two-thirds of these peptides were biological peptides (substrate and target sites of origin listed on the right), most of which displayed higher phospho-activity. BH, Benjamini-Hochberg.
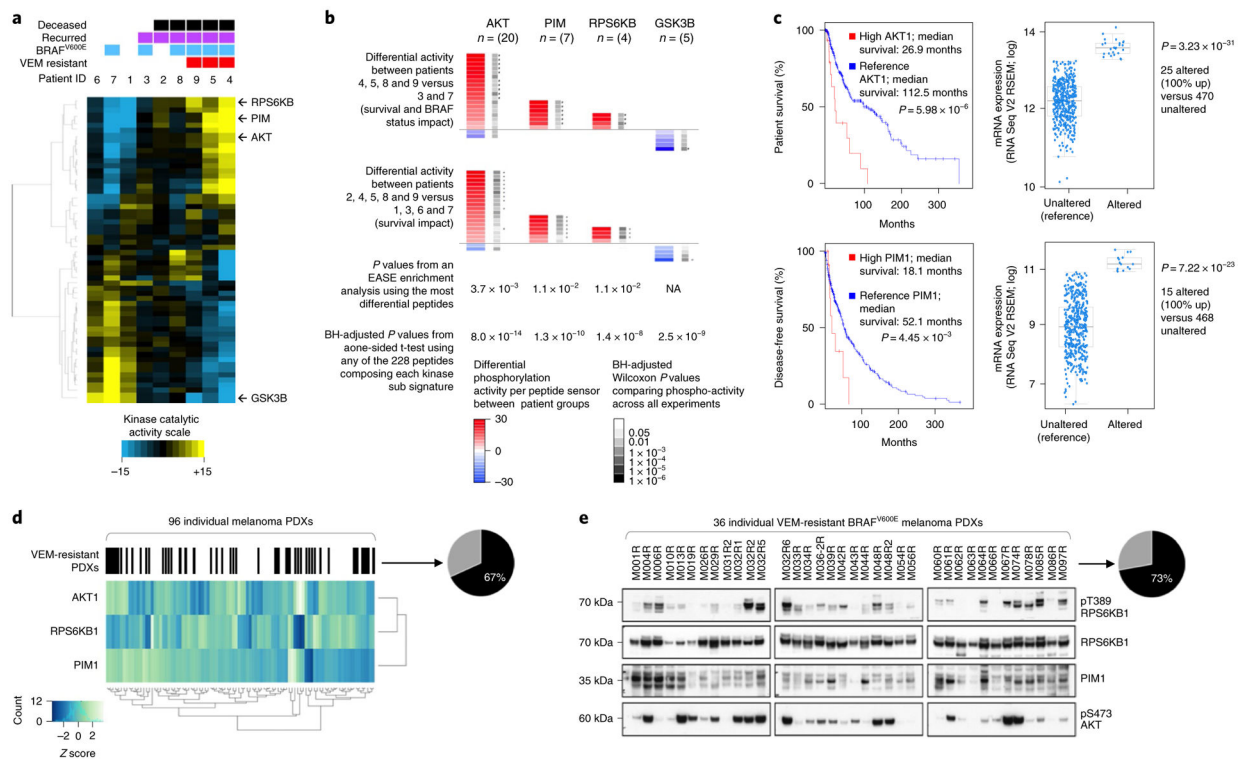
Fig. 7 |. The phospho-catalytic signatures of tumours reveal kinase activities associated with poor outcome and unresponsiveness to VEM in melanoma patients.

a, Kinase activity signatures of tumour tissues *(n = 9* patients; n = 60 kinases). Analysis followed the same steps used to deconvolute the profiles of cell lines. For each tumour, the activity of kinases was calculated as the average of phosphorylation activities measured in presence of their respective biological peptide subsets (kinases detected with > 4 independent biological peptides are shown). Kinase activity profiles were mean-centred per tumour and then per kinase across samples, and color-coded as a blue-to-black-to-yellow scale of relative low-to-medium-to-high activity (in nM ATP). Kinases indicated by an arrow underline the balance between the up-/down-activation of proto-oncogenic kinases (RPS6KB, PIM and AKT) and tumour suppressor kinase (GSK3B) within a patient (top versus bottom) or between patients/patient groups (left versus right). **b**, Sub-heat maps and significance levels of biological peptide phosphorylation activity signatures for AKT, PIM, RPS6KB and GSK3B. Significance values were calculated either by enrichment analysis (EASE; that is, a Fisher's one-sided test using the 34 most differentially phosphorylated peptides associated with survival outcome out of the 228-peptide sensors (see Fig. 6d)) or from FDR-corrected, one-sided Student's f-tests using all (unselected) biological peptides per kinase and comparing all experimental runs between surviving and deceased groups. Dots indicate that a biological peptide was identified among the top 25% most differential phospho-activities. NA, not applicable. **c**, Kaplan-Meier curves (left; log-rank test Pvalues) and enrichment analyses (right; derived from one-sided Student's f-tests; box edges represent the 25th and 75th percentiles, the central line is the median, and whiskers represent the 25th and 75th percentiles+ 1.5x the IQR) for AKT1 (top; n = 4 4 5 patients) and PIM1 (bottom; n = 402 patients) using the TCGA resource. High AKT1 and PIM1 levels are poor

prognosis factors. mRNA, messenger RNA. **d**, RNA-Seq data from 96 melanoma PDXs (Supplementary Table 26). A lighter *z*-score colour indicates higher expression (compared across all PDX profiles). Black bars indicate patients/PDX models resistant to BRAF therapy. The pie chart displays the percentage of VEM-resistant PDXs with a zscore> 0.5 for either AKT1, RPS6KB1 or PIM1 in VEM-resistant PDXs, which was then validated using a chi-squared test comparing gene expression profiles across PDXs (X2< 0.0074). **e**, Protein levels in the 36 BRAF therapy-resistant PDXs (Supplementary Fig. 9) (n = 1 per PDX). The pie chart displays the percentage of VEM-resistant PDXs with an above-average intensity across all tumours for either pAKT1, pRPS6KB1 or PIM1.
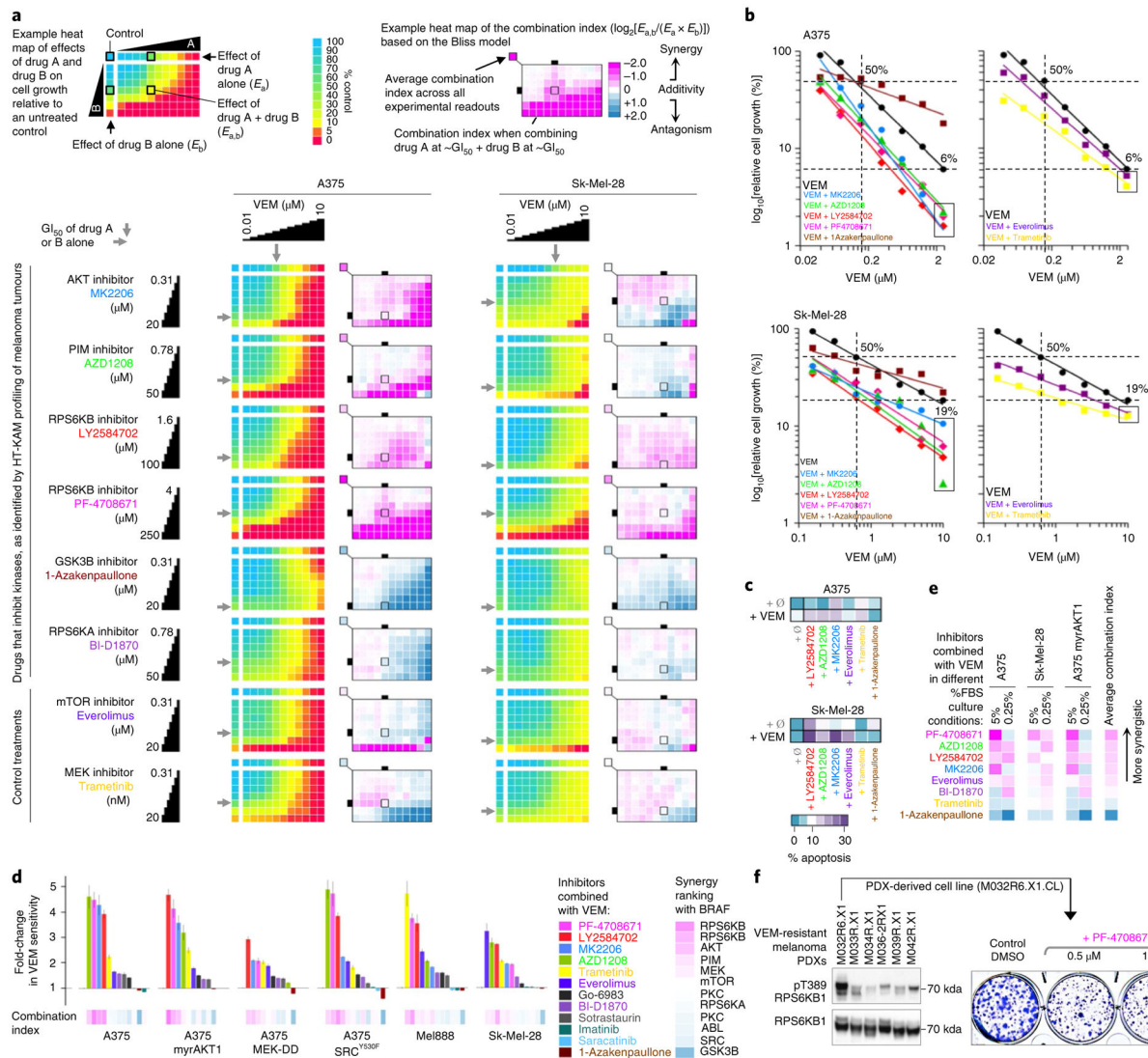
Fig. 8 |. Responses of BRAF^V600E melanoma cell lines, oncogenic mutant models and therapy-resistant PDX-derived cells to drug combinations.

a, Effects of kinase inhibitor combinations on A375 and Sk-Mel-28 cells. To test whether the phospho-catalytic signatures of tumours predictive of poor outcome and VEM unresponsiveness in BRAF^V600E patients (Fig. 7) could also help reveal druggable kinase dependencies, we tested the sensitivity of cell line models to multiple drug combinations. Top, details of the methods and colour scales. Bottom, results from three-day survival assays for cells maintained in 5% FBS media and treated with a range of VEM concentrations (x axis) combined with a second inhibitor (y axis) (n > 3). Growth responses to mTOR/MEK inhibitors are included as positive controls. Sk-Mel-28 cells are inherently highly resilient to BRAF therapy. **b**, Streamlined side-by-side comparison of drugs' effects on cells' responses to BRAF^V600E targeting. Graphs show the percentage of growth inhibition (y axis) resulting from combining VEM at various concentrations (x axis) with a second inhibitor at its GI_{50} concentration alone. Rectangles highlight the highest achievable response elicited by these drug combinations. **c**, Percentage cell death at GI_{50} concentrations measured by

fluorescence-activated cell sorting. **d**, Response to VEM plus a second kinase-targeting drug in different cell models. Waterfall plots (means± s.e.) are sorted by highest to lowest relative change in growth inhibition effect per cell model compared with VEM alone. Measurements were taken at the respective GI50, $GI_{50} \times 2$ and $GI_{50} \times 0.5$ concentrations of each drug in 5% FBS culture (the results were calculated from nine separate drug treatment conditions measured in n > 2 independent experiments; Supplementary Table 26). The individual combination indices across the six cell models and per drug combination (provided underneath the bar graphs) were then averaged, and results are shown to the right (sorted top to bottom from most synergistic to most antagonistic, along with kinase names and inhibitors). The 12 kinase-targeting drug combinations with VEM are listed to the right. **e**, Ranked treatment effects by comparison of the combination index values between melanoma cells. Data from all drug concentration ranges and culture conditions displayed in Fig. 8a and Supplementary Fig. 8a,g are included. **f**, Primary tumour cells derived from a VEM-resistant melanoma PDX displaying high levels of phospho-RPS6KB1 protein (used as a readout of kinase activity) are sensitive to a RPS6KB-targeting drug in a three-week colony formation assay (n = 1). DMSO, dimethyl sulfoxide.